Copyright Warning & Restrictions

The copyright law of the United States (Title 17, United States Code) governs the making of photocopies or other reproductions of copyrighted material.

Under certain conditions specified in the law, libraries and archives are authorized to furnish a photocopy or other reproduction. One of these specified conditions is that the photocopy or reproduction is not to be "used for any purpose other than private study, scholarship, or research." If a, user makes a request for, or later uses, a photocopy or reproduction for purposes in excess of "fair use" that user may be liable for copyright infringement,

This institution reserves the right to refuse to accept a copying order if, in its judgment, fulfillment of the order would involve violation of copyright law.

Please Note: The author retains the copyright while the New Jersey Institute of Technology reserves the right to distribute this thesis or dissertation

Printing note: If you do not wish to print this page, then select "Pages from: first page # to: last page #" on the print dialog screen

Conditional Artificial Dielectrics: Fabry-Perot Etalon

Ling-Yi Hu

Department of Electrical Engineering

New Jersey Institute of Technology

December 1991

Approval Sheet

Title of Thesis: Conditional Artificial Dielectrics; Fabry-Perot Etalon

Name of Candidate: Ling-Yi Hu

Master of Science in Electrical Engineering

Thesis and Abstract Approved: _____ _____

Dr. Haim Grebel Date 12/19/91

Professor in Department of Electrical Engineering

New Jersey Institute of Technology, Newark, N.J.

_____ _____

Dr. Marek Sosnowski Date 12/19/91

Professor in Department of Electrical Engineering

New Jersey Institute of Technology, Newark, N.J.

_____ _____

Dr. Kenneth Sohn Date 12/19/91

Professor in Department of Electrical Engineering

New Jersey Institute of Technology, Newark, N.J.

Contents

Abstract

Fabry-Perot etalons are optical resonators comprise of two mirrors and a spacer layer. By embedding a thin, photo-sensitive layer (Conditional Artificial Dielectric - CAD layer) in the middle of the spacer layer, we were able to photo-control the transmission properties of a Fabry-Perot etalon. Different structures have been analyzed and measured to find that a change of .01 was photo-activated in the refractive index of the Conditional Artificial Dielectric layer.

1 Introduction

Fabry-Perot interferometer – the multiple-beam interferometer, first constructed by Charles Fabry and Alfred Perot in the late eighteen hundreds, is of considerable importance in modern optics and is frequently used to examine the details in spectroscopic lines. Its particular value arises from the fact that besides being a spectroscopic device of extremely high resolving power, it also serves as the basic laser resonant cavity. In principle, the device consists of two plane, parallel partially reflecting surfaces facing each other which are separated by some distance l. In practice, the two partially reflecting surfaces can be metallic layers or multilayer dielectrics coatings. (Figure 1). Typically, the spacer layer of a Fabry-Perot etalon is air. If the distance between the mirrors is changed and thus the effective optical path between them is changed , then the position of the resulting transmission peaks changes too. Moreover, only certain well defined wavelengths will be transmitted through the device at a given thickness of spacer layer l and an incident angle θ.

As the incident rays pass through the partially reflecting mirror, they will be reflected back and forth in the spacer layer between the two mirrors. Some of the

light will emerge from the spacer at every reflection. If the optical phase delay of succesive emerging "rays" is equal to an integral number of 2π, then the transmitting rays will have constructive interference. In view of Wavelength Division Multiplexing schemes, changing the optical path between the two mirrors may be made by other means than merely changing the distance l or the incident angle θ. For example, one may use a nonlinear material as a spacer material, or, as was done in this thesis, embed a very thin, photosensitive layer in the middle of the spacer layer to control the phase of the transmitted beam as shown in Figure 2. The photosensitive layer is made by embedding small clusters of semiconductor material, such as CdS within a polymeric spacer.

Transmission mode of Fabry-Perot devices has been recognized to be useful in interference filters and has found applications in a number of optical systems. [1] For example, we can use a thin film Fabry-Perot as a narrowband filter whose structure is the same as shown in Fig. 1. For a collimated light, the transmission is very low for most wavelengths except for a series of narrow spectral bands that are constant in terms of wavenumber. There is another thin film filter, with higher efficiency and higher rejection ratio, which can be obtained by substituting

multiple dielectric layers for the metallic reflection layers. The dielectric reflecting layers exhibit very low absorption and therefor facilitate higher reflectance values at a given transmittance level.

The mirrors of Fabry-Perot etalon do not have to be plane. Sometimes spherical mirrors will improve the performane of the Fabry-Perot etalon. Owing that the Fabry-Perot etalon is very sensitive to the phase change , it can be used as a spectrometer. Plane mirrored Fabry-Perot spectrometer is limited in resolution as only a finite range of the angle of incidence for the incoming light can be usefully employed. [2] Instead a spherical mirrored Fabry-Perot may be used to increase the device spectral resolution. The spherical Fabry-Perot device consists of two sperical mirrors which are seperated by a distance which is the sum of radii of curvature of the mirrors. This results in interferometric high resolution device which accomodates large range of the angle of incidence of the incoming light. [3]

Artificial dielectrics are dielectrics in which other dielectrics are embedded to achieve desired dielectric properties different from the properties of the compounds. [4][5] Guest-host polymeric structures for integrated optics have gained interest re-

cently since they offer flexibility in fabrication and have potential as novel dielectric materials. Conditional Artificial Dielectrics (CAD) are semiconductor clusters embedded in a passive host material. Upon illumination the CAD material with photons having energy above the bandgap energy of the semiconductor clusters (pump beam), the dielectric properties of this layer will change due to the induction of electric and magnetic dipoles. This dielectric changes may be detected when another optical beam, with photon energy lower than the energy bandgap of the semiconductor clusters, is transmitted through the Fabry-Perot etalon, under illumination of the pump beam. We obtained a conditional artificial layer by embedding a CdS thin film within a polymethyl methacrylate (PMMA) spacer layer (see Figure 2). The Conditional Artificial Dielectric layer, CdS thin film, embedded in the PMMA can be treated as a multi-dielectric structure; the CdS layer is very thin, so we can neglect the multiple reflection within this layer.

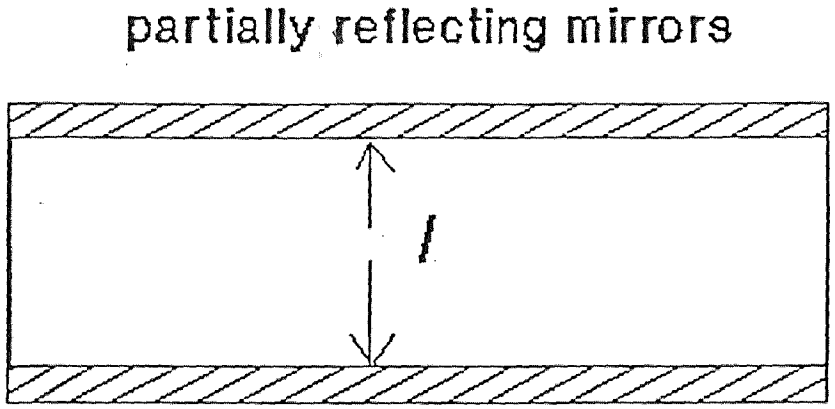

Figure 1 The structure of regular Fabry-Perot etalon.

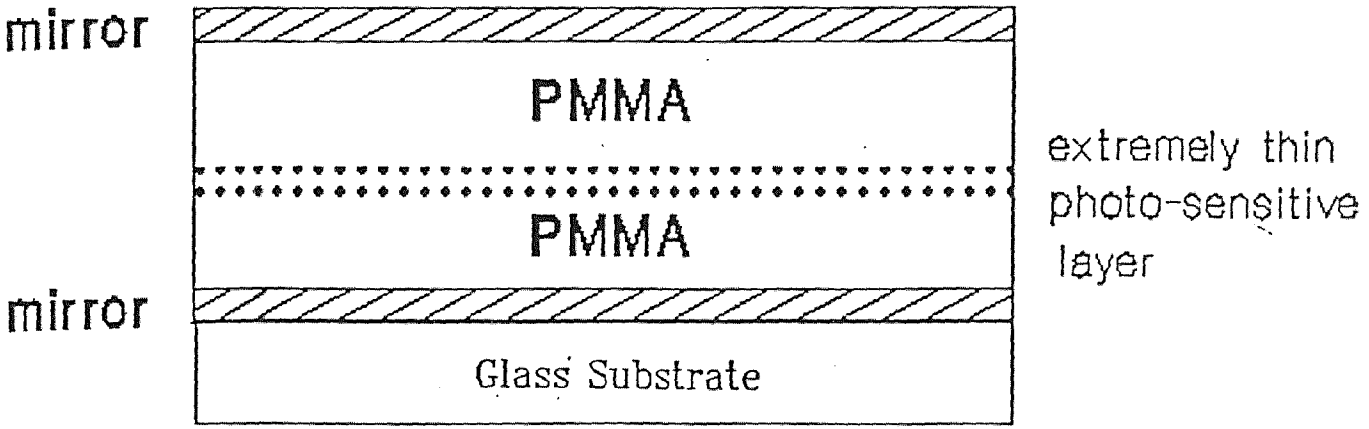

Figure 2 The structure of conditional artificial dielectrics Fabry-Perot etalon.

The mirrors are made by depositing a thin film of aluminium.

In order to demonstrate its properties, we used light from a He-Ne laser which has a photon energy below the bandgap of the CdS clusters. Upon illumination with another beam of light with photons having larger energy than the bandgap of the

CdS material, dipoles are generated in the CdS clusters. Under these conditions the photon-sensitive layer affects the path of light with low energy photon through the etalon. In this experiment, we used a light with wavelength $\lambda = .6328\mu m$ from a He-Ne laser, and variable angle of incidence to measure the transmission intensity profile of a Fabry-Perot etalon.

In this thesis, the theory and experimental results for standard and conditional artificial dielectrics Fabry-Perot etalons will be presented. In Chapter 2, the theory of two-mirror and multimirror Fabry-Perot interferometer is described. Thin film deposition system and the experimental results are described in Chapter 3 and Chapter 4, respectively. The discussion of experimental results is in Chapter 5 and Conclusion in Chapter 6.

2 Analysis of Fabry-Perot Etalon

Etalons used to measure fractional shifts in spectral lines require very accurate specification of their transmission functions. In this chapter, we introduce the theory of a standard Fabry-Perot etalon, CdS embedded Fabry-Perot etalon and consider losses due to light absorption in these materials.

2.1 Two-mirror Fabry-Perot Etalon

In this section, we consider an ideal Fabry-Perot etalon . It consists of a plane parallel plate of thickness l and an index of refraction n which is sandwitched between two mirrors. We consider two cases (a) Etalon sandwitched between two mirrors having the same reflection coefficient (b) Etalon having two dissimilar mirrors.

I. ETALON WITH THE SAME MIRRORS

A plane wave denoted by S is incident upon the etalon at an angle $0'$ as shown in Figure 3. At each interface, that is , at each of the two partially reflecting mirrors, some light is reflected and some is transmitted through the interface. The total

reflected light comprises of all the light " rays " reflected from the device, that is, the sum of $B_1 + B_2 + B_3 + ...$ etc. The total transmitted light is the sum of all " rays " which pass through the device, that is , $A_1 + A_2 + A_3 + ...$ etc.

The phase delay between two waves emerging from a given interface is attributed to the differences in phase. In the experiment, one varies the phase by rotating the sample with respect to the incident laser beam. Their optical path as can be seen from Figure 4 the phase delay δ between the waves with amplitudes A_1 and A_2 depends on the incident angle $0'$ [14],

$$\delta L = \overline{AB} + \overline{BC} = \frac{l}{cos\theta} + \frac{lcos2\theta}{cos\theta} = 2lcos\theta. \qquad (1)$$

The corresponding phase difference is,

$$\delta = \frac{2\pi(\delta L)n}{\lambda} = \frac{4\pi nlcos\theta}{\lambda}. \qquad (2)$$

Where λ is the vacuum wavelength of the incidence wave, 0 is the internal angle of incident and n is the refractive index of the spacer layer and l is the distance between the mirrors.

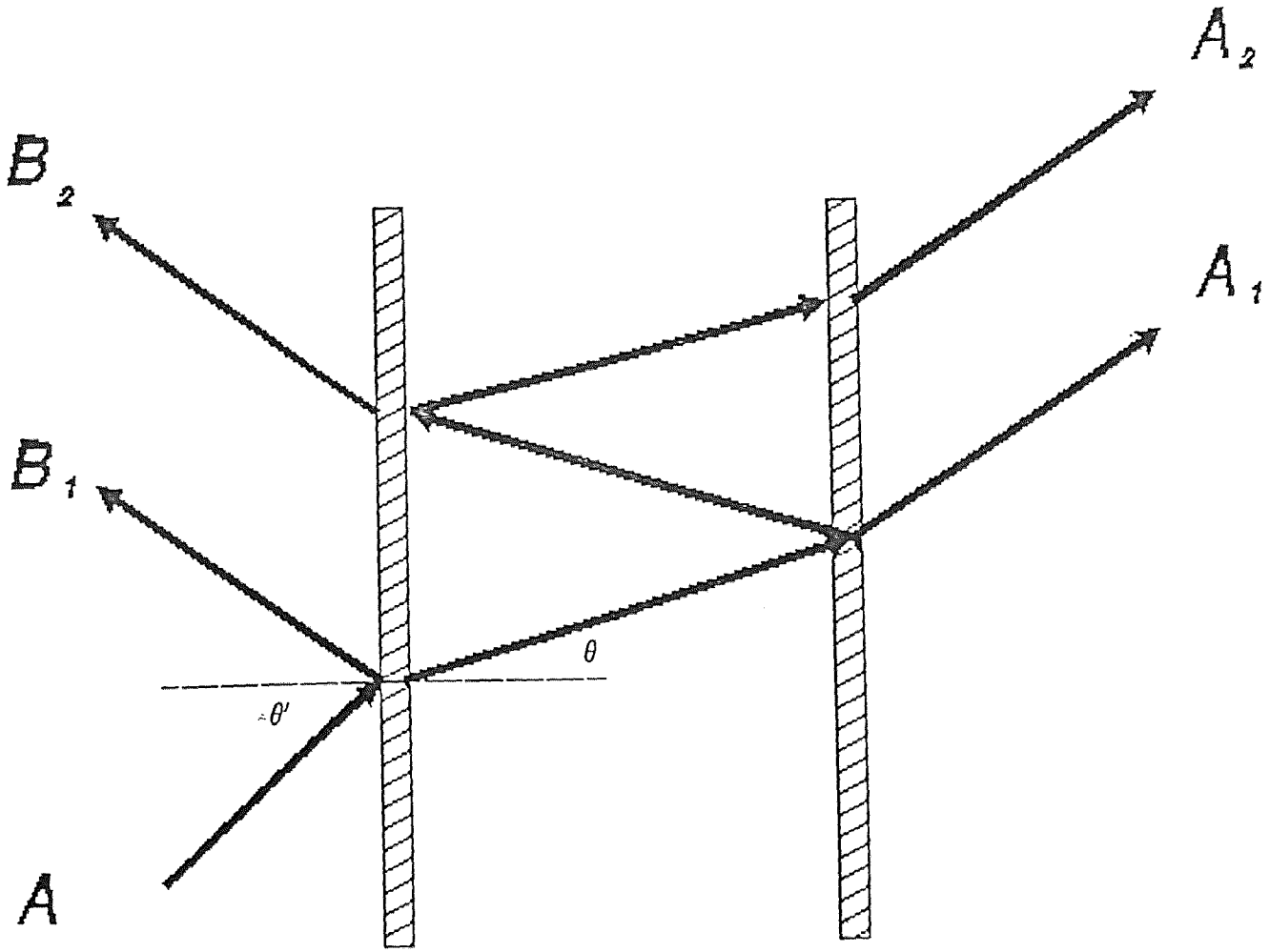

Figure 3 Multiple reflection in Fabry-Perot .

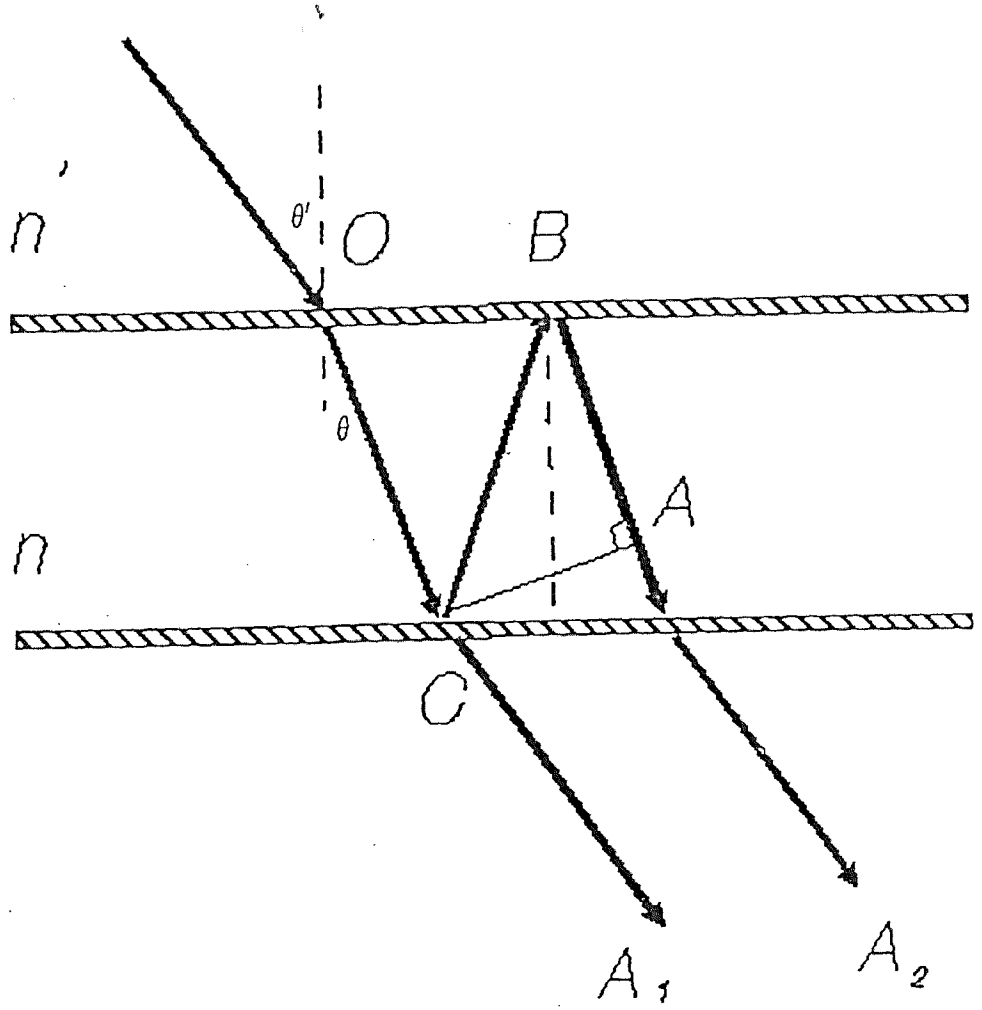

Figure 4 The path difference between two successive reflection A_1 and A_2.

According to Fig. 3, some of the incident light S , is reflected into the ray B_1. Let A be the amplitude of the incident ray. If r and t are the reflection and transmission coefficients at each mirror as approached from outside of the spacer layer, r' and t' are the corresponding quantities from the spacer layer to two mirrors, we can write down the amplitudes of the reflected rays as.

$$B_1 = rA,\ B_2 = tt'r'Ae^{i\delta},\ B_3 = tt'r'^3Ae^{2i\delta},\ B_4 = tt'r'^5Ae^{3i\delta}, \ldots . \tag{3}$$

and the amplitudes of the transmitted rays as,

$$A_1 = tt'A,\ A_2 = tt'r'^2Ae^{i\delta},\ A_3 = tt'r'^4Ae^{2i\delta},\ A_4 = tt'r'^6Ae^{3i\delta}, \ldots . \tag{4}$$

The total reflected wave is $A_r = B_1 + B_2 + B_3 + B_4 + \ldots$

$$\begin{aligned} A_r &= rA + tt'r'Ae^{i\delta} + tt'r'^5Ae^{2i\delta} + tt'r'^5Ae^{3i\delta} + \ldots . \\ &= \{r + tt'r'e^{i\delta}(1 + r'^2e^{i\delta} + r'^4e^{2i\delta} + \ldots)\}A, \end{aligned} \tag{5}$$

The total transmitted wave is $A_t = A_1 + A_2 + A_3 + \ldots$

$$A_t = tt'A + tt'r'^2Ae^{i\delta} + tt'r'^4Ae^{2i\delta} + \ldots$$

$$= tt'(1 + r'^2e^{i\delta} + r'^4e^{2i\delta} + \ldots)A. \tag{6}$$

Considering lossless mirrors, $r' = -r$. Conservation of energy dictates,

$$r^2 + tt' = 1. \tag{7}$$

With the definitions,

$$R = r^2 = r'^2 \qquad T = tt'. \tag{8}$$

Where R and T are the light reflected and transmitted intensities from the mirrors respectively. We can write A_r and A_t as,

$$A_r = [\sqrt{R} + (1 - R)\sqrt{R}e^{i\delta}\frac{1}{1 - Re^{i\delta}}]A. \tag{9}$$

and

$$A_t = [\frac{T}{1 - Re^{i\delta}}]A. \tag{10}$$

The transmission of a Fabry-Perot etalon is as follow:

$$\frac{I_t}{I_i} = \frac{A_t A_t^*}{AA^*} = \frac{T^2}{(1-R)^2 + 4Rsin^2(\frac{\delta}{2})}. \tag{11}$$

and the total reflectivity is,

$$\frac{I_r}{I_i} = \frac{A_r A_r^*}{AA^*} = \frac{4Rsin^2(\frac{\delta}{2})}{(1-R)^2 + 4Rsin^2(\frac{\delta}{2})}. \tag{12}$$

where $\delta = 4\pi nlcos\theta/\lambda$ as before.

According to Eq. 11, the transmission will become unity if,

$$\delta = \frac{4\pi nlcos\theta}{\lambda} = 2m\pi \qquad with\ m = any\ integer. \tag{13}$$

here n = the refractive index of spacer layer ($\approx$ 1.5 in our experiments), l is the thickness of spacer layer and λ is the incident wavelength ($\approx 0.6328\mu m$ for a He-Ne laser). Figure 5 shows the intensity transmission

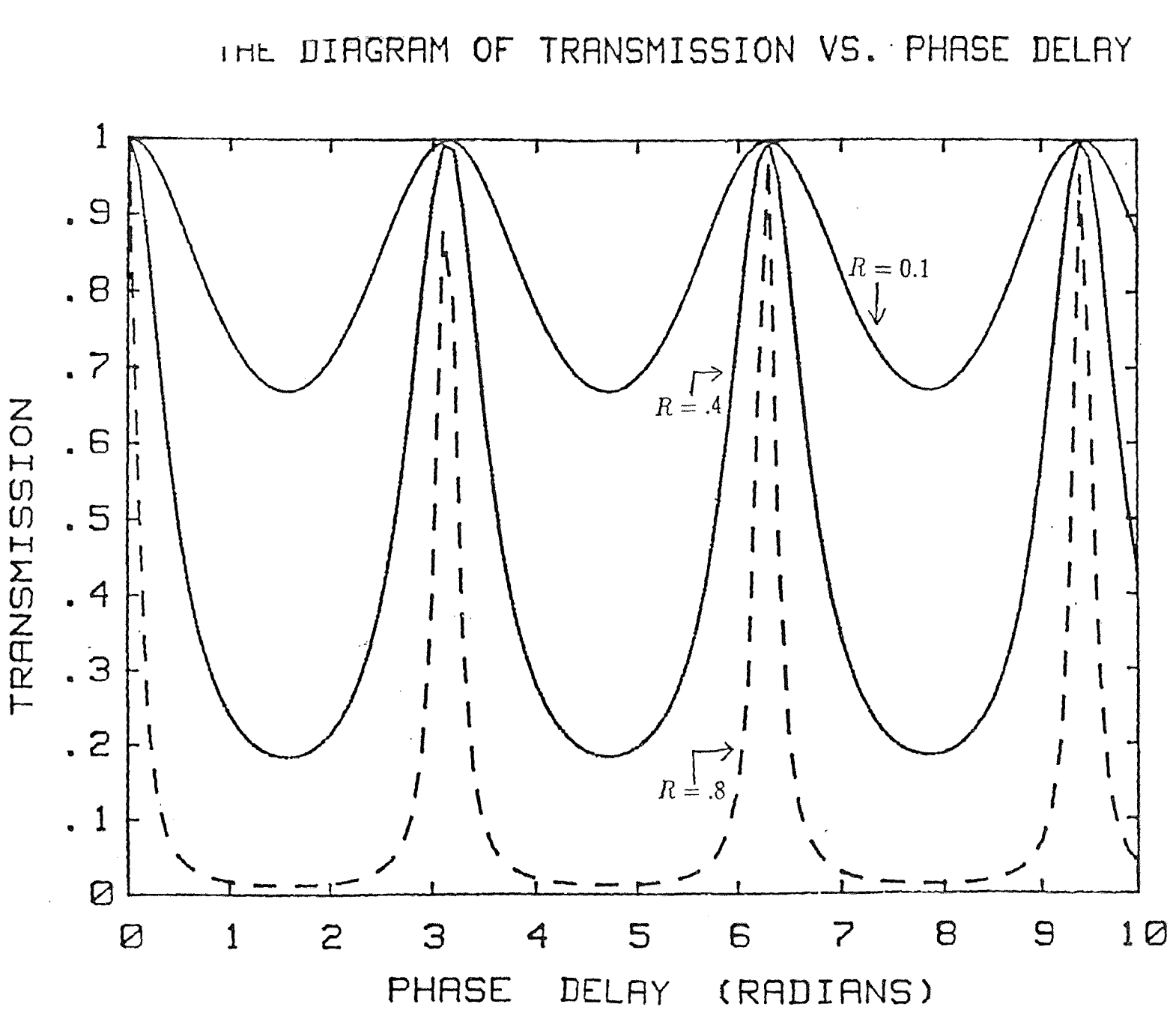

Figure 5 The relation of transmission and phase length (δ / 2) for different R ($R_1 = R_2 = R$).

profile of an ideal Fabry-Perot etalon with the mirrors having the same reflectivity.

The transmission may be written with the help of Fresnel coefficient F:

$$\frac{I_t}{I_i} = \frac{1}{1 + F sin^2(\frac{\delta}{2})}. \tag{14}$$

where

$$F = \frac{4R}{tt'} = \frac{4R}{(1-R)^2}. \tag{15}$$

The parameter F becomes large when R approaches unity. Figure 6 is a plot of I_t/I_r for several values of F.

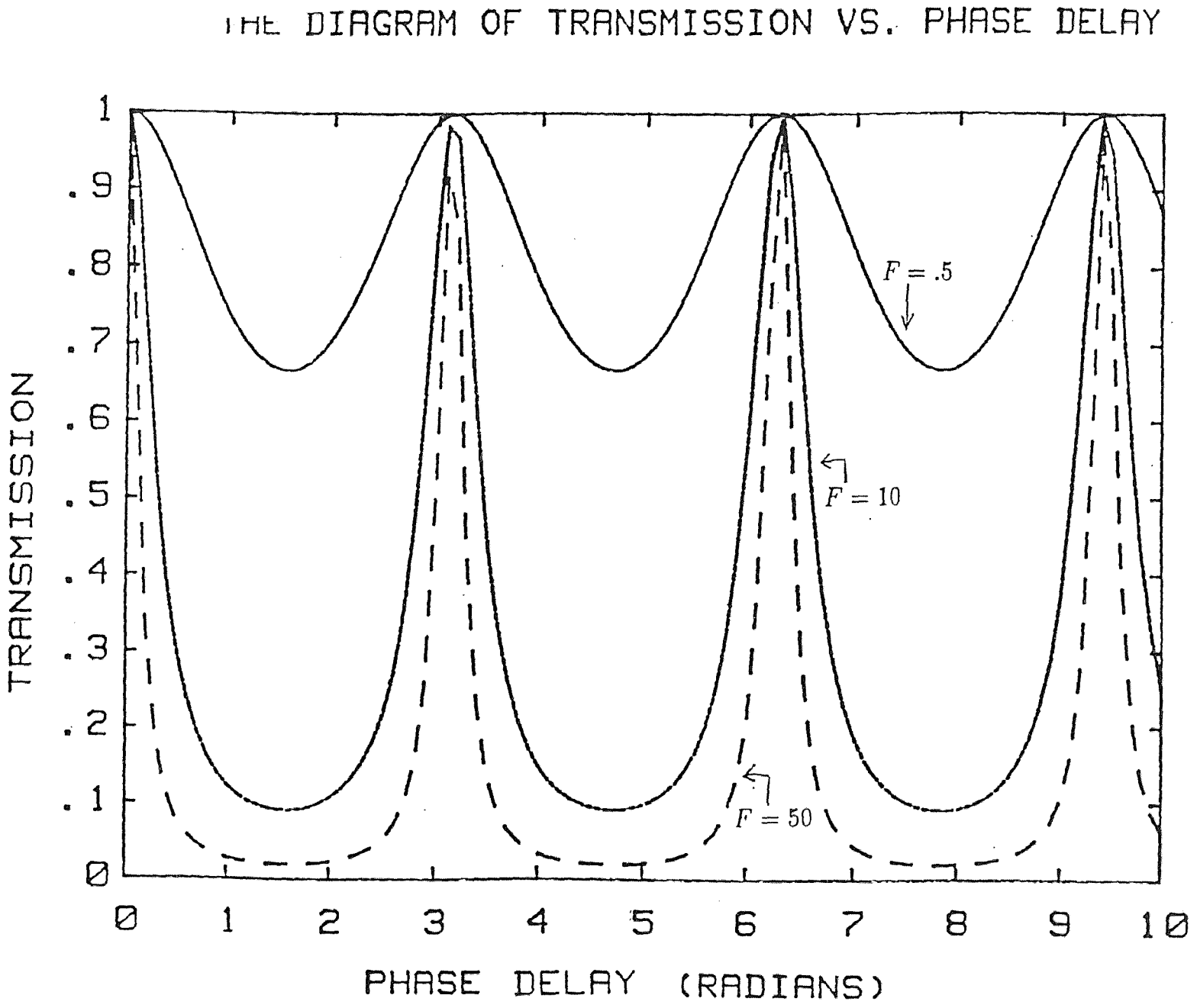

Figure 6 The relation of transmission and phase length (δ / 2) for different F.

II. ETÁLON WITH MIRRORS HAVING DIFFERENT REFLECTIVITIES

We will consider an incident angle $\theta = 0$ case for simplicity. From Figure 7, E_1^+ and E_2^+ are the amplitudes of the electric field vector of the wave incident on the left-hand side of mirrors 1 and 2 respectively. E_1^- and E_2^- are the electric field amplitudes of the reflected optical wave traveling to left. The coefficients r_1, r_2 and t_1 , t_2 are the reflection and transmission coefficients of mirror 1 and 2 respectively. The distance between two mirrors is l, , and the total phase delay of an optical beam traveling in the spacer layer in a perpendicular direction is $\phi = 2\pi l/\lambda$.

Then we find the relations between the electric fields E_1 and E_2 as,

$$E_2^+ e^{-i\phi} = t_1 E_1^+ + r_1 E_2^- e^{+i\phi}. \tag{16}$$

$$E_1^- = -r_1 E_1^+ + t_1 E_2^- e^{+i\phi}. \tag{17}$$

Where $\phi = \frac{2\pi l}{\lambda}$ is the phase delay.

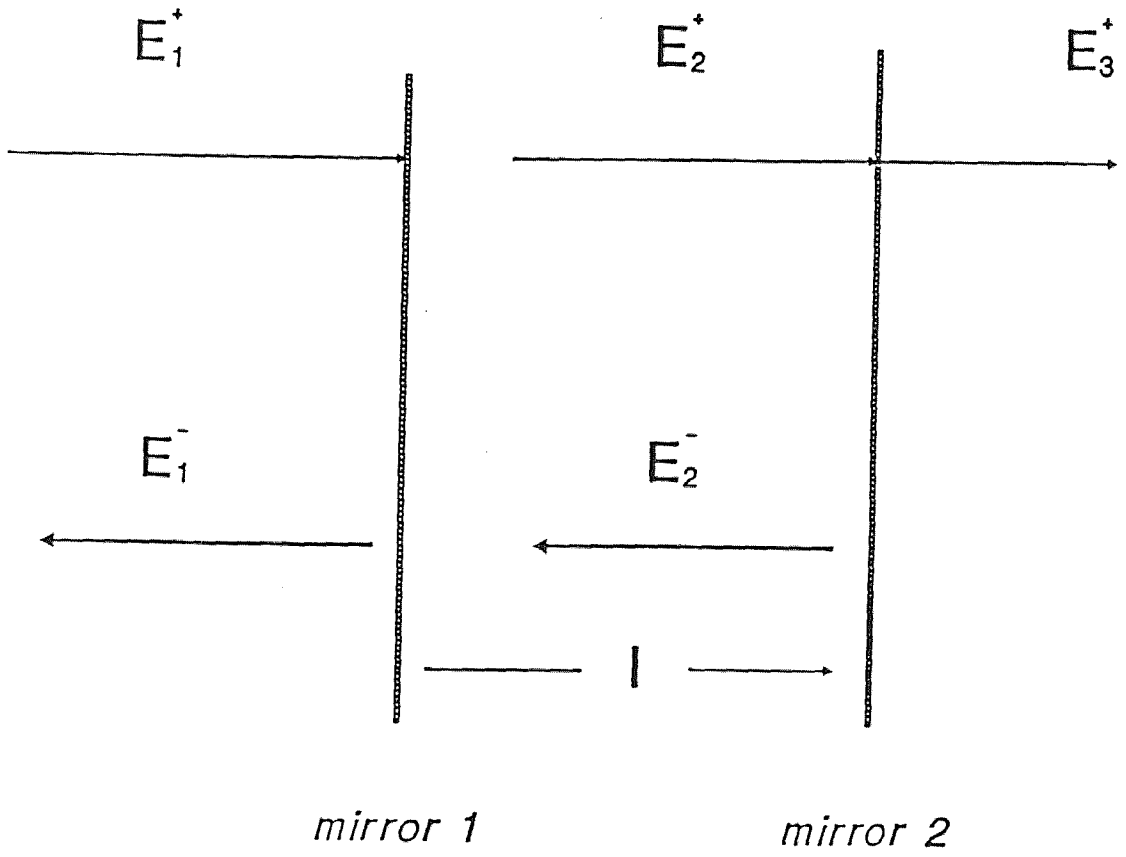

Figure 7 The amplitudes at mirror 1 and 2 out of two-mirror Fabry-Perot etalon.

Using $r^2 + t^2 = 1$ as before, and eliminating E_1^+ from Eq. 16 and Eq. 17 , we can get,

$$E_1^- = -\frac{r_1}{t_1} E_2^+ e^{-i\phi} + \frac{1}{t_1} E_2^- e^{+i\phi}. \tag{18}$$

Rewriting Eq. 16 as,

$$E_1^+ = \frac{1}{t_1} E_2^+ e^{-i\phi} - \frac{r_1}{t_1} E_2^- e^{+i\phi}. \tag{19}$$

From Eq. 18 and Eq. 19 , we can write the relations of the E_1 and E_2 in matrix form,

$$\begin{bmatrix} E_1^+ \\ E_1^- \end{bmatrix} = \frac{1}{t_1} \begin{bmatrix} e^{-i\phi} & -r_1 e^{+i\phi} \\ -r_1 e^{-i\phi} & e^{+i\phi} \end{bmatrix} \begin{bmatrix} E_2^+ \\ E_2^- \end{bmatrix} \tag{20}$$

The transmission coefficient t is found as,

$$t = \frac{E_3^+}{E_1^+} = \frac{t_2 E_2^+}{E_1^+} = \frac{t_2 E_2^+}{\frac{1}{t_1}[E_2^+ e^{-i\phi} - r_1 E_2^- e^{+i\phi}]}$$

$$(E_2^- = -r_2 E_2^+)$$

$$= \frac{t_1 t_2 E_2^+}{E_2^+ e^{-i\phi} + r_1 r_2 E_2^+ e^{+i\phi}} = \frac{t_1 t_2}{e^{-i\phi} + r_1 r_2 e^{+i\phi}}. \tag{21}$$

The transmission T of a Fabry-Perot etalon is,

$$T = tt^* = \frac{t_1^2 t_2^2}{1 + r_1^2 r_2^2 + 2r_1 r_2 cos(2\phi)}.$$

Let $r_1 = r_2 = r$ and $t_1 = t_2 = t$. Eq. (22) becomes,

$$\begin{aligned} T &= \frac{t^4}{1 + r^4 + 2r^2 cos(2\phi)} \\ &= \frac{t^4}{1 + r^4 - 2r^2 + 4r^2 cos^2(\phi)} \\ &= \frac{t^4}{(1 - r^2)^2 + 4r^2 cos^2(\phi)}. \end{aligned} \tag{23}$$

$$with\ cos(2\phi) = cos^2\phi - sin^2\phi = 2cos^2\phi - 1.$$

The transmission can be unity, provided that,

$$cos\phi = 0 \implies \phi = (m + 1/2)\pi. \tag{24}$$

and, thus, we get the same results obtained before for two similar mirrors.

2.2 Multi-interface Fabry-Perot Etalon

CdS-embedded Fabry-Perot is shown in Figure 2. It comprises of two partial mirrors, as before, with the addition of a thin semiconductor cluster layer embedded in the midst of the etalon. The thickness of this layer is very small compared to the etalon spacing l. We will treat the Fabry-Perot etalon, the CdS Conditional Artificial Dielectric layer, as a device with three reflecting surfaces. We justify our approach by two reasons:

1. The layer is inhomogeneous and consists of CdS clusters. These clusters, which are assumed to have dimensions smaller than the optical wavelength, effectively make the refractive index of this layer different from that of the polymeric spacer. Thus reflection occurs at the interface between this layer and the spacer material.

2. The layer thickness is small (or the order of .1 μ m) compared to the etalon spacer $l \cong 10\mu m.$ or more. Thus, it may be treated as an interface rather than a bulk layer.

The method of analysis is the same as we used in part II of section 2-1. Schematic cross section showing the reflected and transmitted beams is given in Figure 8.

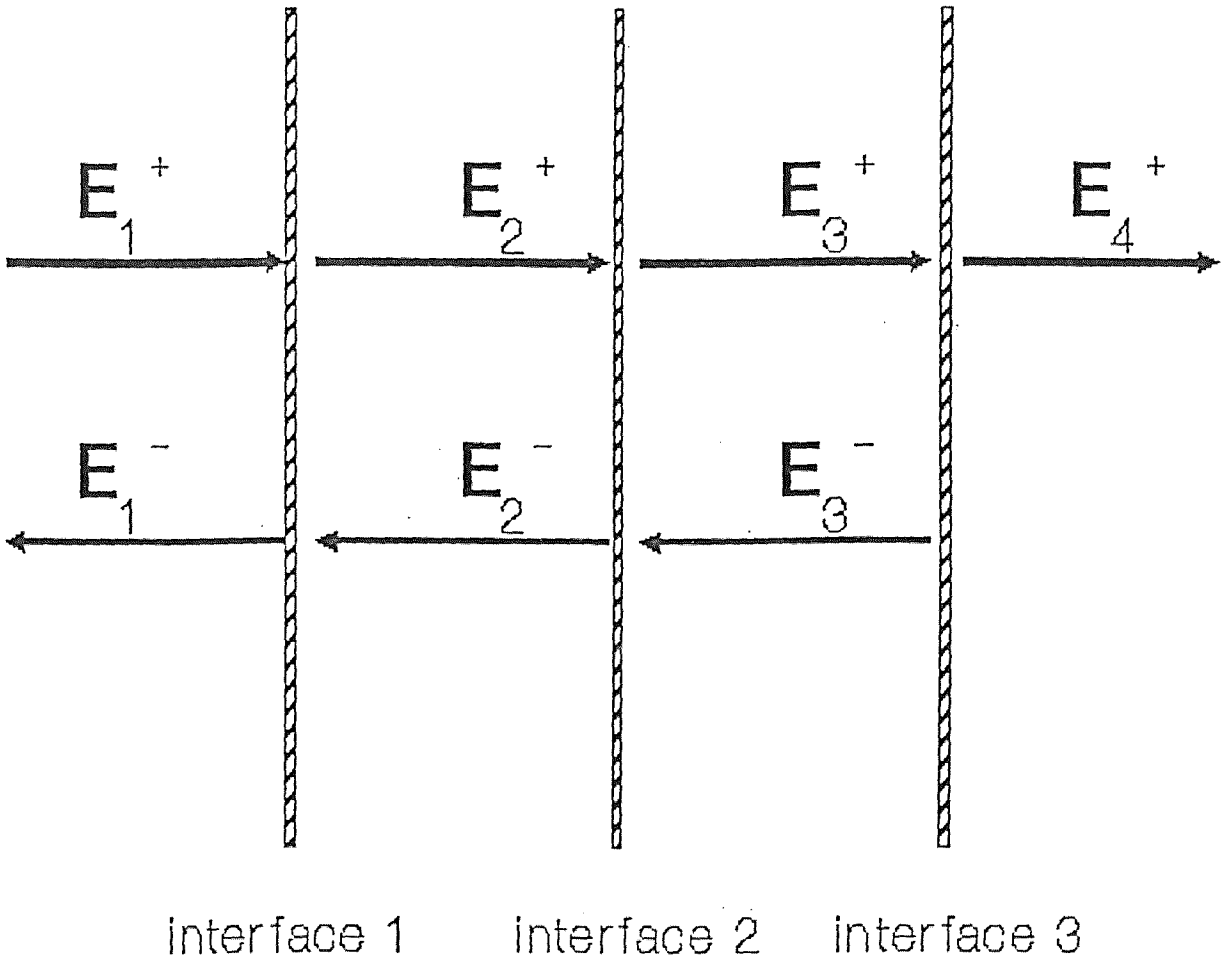

Figure 8 The amplitute at interface 1 , interface 2 and interface 3 out of three-interface Fabry-Perot etalon.

We can rewrite Eq. 16 and Eq. 17 as(for metallic interfaces),

$$E_{i+1}^{+} e^{-i\phi_i} = t_i E_i^{+} + r_i E_{i+1}^{-} e^{+i\phi_i} \tag{25}$$

$$E_i^{-} = -r_i E_i^{+} + t_i E_{i+1}^{-} e^{+i\phi_i} \tag{26}$$

Where $i = 1$, 2 or 3 for different interfaces. Eliminating E_i^{+}, and using $r^2 + t^2 = 1$ we can get,

$$E_i^{-} = -\frac{r_i}{t_i} E_{i+1}^{+} e^{-i\phi_i} + \frac{1}{t_i} E_{i+1}^{-} e^{+i\phi_i} \tag{27}$$

Eq. 25 and Eq. 27 can be written in matrix form,

$$\begin{bmatrix} E_i^{+} \\ E_i^{-} \end{bmatrix} = \frac{1}{t_i} \begin{bmatrix} e^{-i\phi_i} & -r_i e^{+i\phi_i} \\ -r_i e^{-i\phi_i} & e^{+i\phi_i} \end{bmatrix} \begin{bmatrix} E_{i+1}^{-} \\ E_{i+1}^{-} \end{bmatrix}. \tag{28}$$

If there are N planes parallel and partially transmitting mirrors, the general result is

$$\begin{bmatrix} E_1^{+} \\ E_1^{-} \end{bmatrix} = \frac{1}{t_1 t_2 \ldots t_{N-1}} \begin{bmatrix} e^{-i\phi_1} & -r_1 e^{+i\phi_1} \\ -r_1 e^{-i\phi_1} & e^{+i\phi_1} \end{bmatrix} \begin{bmatrix} e^{-i\phi_2} & -r_2 e^{+i\phi_2} \\ -r_2 e^{-i\phi_2} & e^{+i\phi_2} \end{bmatrix} \times \ldots \times \begin{bmatrix} e^{-i\phi_{N-1}} & -r_{N-1} e^{+i\phi_{N-1}} \\ -r_{N-1} e^{-i\phi_{N-1}} & e^{+i\phi_{N-1}} \end{bmatrix} \begin{bmatrix} E_N^{+} \\ E_N^{-} \end{bmatrix}. \tag{29}$$

Adding one layer of CdS to a standard Fabry-Perot etalon, results a three-interfaces Fabry-Perot interferometer. The reflection coefficient of the CdS thin film is determined by the indices of refraction of the CdS thin film and polymeric spacer layer. This condition is similar to a multiple dielectric slab structure which has reflection coefficient [17],

$$r_2 \equiv r_{12} = \frac{\eta_2 - \eta_1}{\eta_2 + \eta_1} \tag{30}$$

r_{12} is the input reflection coefficient from medium 1 to medium 2 for normal incident case. If , as expected, the refractive index of polymeric spacer layer is smaller than that of the embedded CdS thin film, then $r_{12} \geq 0$, otherwise, $r_{12} \leq 0$.

The relation in Eq. 29 will be used with N = 3 in the case of $r_2 \leq 0$, gives,

$$\begin{bmatrix} E_1^+ \\ E_1^- \end{bmatrix} = \frac{1}{t_1 t_2} \begin{bmatrix} e^{-i\phi_1} & -r_1 e^{+i\phi_1} \\ -r_1 e^{-i\phi_1} & e^{+i\phi_1} \end{bmatrix} \begin{bmatrix} e^{-i\phi_2} & -r_2 e^{+i\phi_2} \\ -r_2 e^{-i\phi_2} & e^{+i\phi_2} \end{bmatrix} \begin{bmatrix} E_3^+ \\ E_3^- \end{bmatrix} \tag{31}$$

The transmission coefficient is

$$t = \frac{E_4^4}{E_1^+} = \frac{t_3 E_3^+}{E_1^+}$$

$$\frac{t_1 t_2 t_3 E_3^+}{(i\phi_1 - i\phi_2)]E_3^+ + [-r_2 e^{(-i\phi_1)} - r_1 e^{(i\phi_1 + i\phi_2)}]E_3^-}$$

$$(E_3^- = -r_3 E_3^+)$$

$$\frac{t_1 t_2 t_3}{(i\phi_1 - i\phi_2)} + r_2 r_3 e^{(-i\phi_1 + i\phi_2)} + r_1 r_3 e^{(i\phi_1 + i\phi_2)}$$

(32)

lection coefficients and t_1, t_2 and t_3 are the trans-

:s 1, 2 and 3 respectively.

ansmission of light intensity as

(33)

$r_3)^2 + (r_1 r_3)^2 + 2r_1 r_2(1 + r_3^2)cos(2\phi_1)$

$cos(2\phi_2) + 2r_1 r_3 cos(2\phi_1 + 2\phi_2)$

$2\phi_1 - 2\phi_2)$ (34)

n Eq. 32 will reduce to the form of two-mirror

2.

For the case of $r_{12} \geq 0$, Eqs. 31 becomes,

$$\begin{bmatrix} E_1^+ \\ E_1^- \end{bmatrix} = \frac{1}{t_1 t_2} \begin{bmatrix} e^{-i\phi_1} & -r_1 e^{+i\phi_1} \\ -r_1 e^{-i\phi_1} & e^{+i\phi_1} \end{bmatrix} \begin{bmatrix} e^{-i\phi_2} & +r_2 e^{+i\phi_2} \\ +r_2 e^{-i\phi_2} & e^{+i\phi_2} \end{bmatrix} \begin{bmatrix} E_3^+ \\ E_3^- \end{bmatrix} \tag{35}$$

The transmission coefficient is,

$$t = \frac{t_1 t_2 t_3}{e^{(-i\phi_1 - i\phi_2)} - r_1 r_2 e^{(i\phi_1 - i\phi_2)} - r_2 r_3 r^{(-i\phi_1 + i\phi_2)} + r_1 r_3 e^{(i\phi_1 + i\phi_2)}} \tag{36}$$

The expression of Eq. 34 becomes,

$$\begin{aligned} D = 1 &+ (r_1 r_2)^2 + (r_2 r_3)^2 + (r_1 r_3)^2 - 2r_1 r_2(1 + r_3^2)cos(2\phi_1) \\ &-2r_2 r_3(1 + r_1^2)cos(2\phi_2) + 2r_1 r_2 cos(2\phi_1 + 2\phi_2) \\ &+2r_1 r_2^2 r_3 cos(2\phi_1 - 2\phi_2) \end{aligned} \tag{37}$$

Figures 9a to 11b show the transmission of the intensity pattern when the mirror reflectivities r_1, r_2 and r_3 and the phase delays ϕ_1, ϕ_2 are varied.

Figures 9a, 10a and 11a show the resulting transmission for the case of $r_{12} \leq 0$ (using Eqs. 33 and 34). Figures 9b, 10b and 11b are for the case of $r_{12} \geq 0$ (using

Eq. 36 and 37). As can be seen from Fig. 9a and 9b maxima of the two split peaks get closer as the reflectivity of the middle interface becomes larger. These double peaks become a single peak as in a regular Fabry-Perot etalon. Figure 10a and 10b show the relation of intensity transmssion of three-mirror Fabry-Perot with different phase delay of spacer layer 1 and 2, ϕ_1 and ϕ_2, and also differnet reflectivities of mirrors 1 and 2 . Comparing Figs. 10a, 10b and Figs. 9a, 9b, we can see that the shape of Figs. 10a and 10b, are not symmetrical with respect to the split peaks. Also, the peaks' position changes as the reflectivity of middle mirror is changed. Figs. 11a and 11b shows that if the difference in the phase lengths of the spacer layer 1 and spacer layer 2

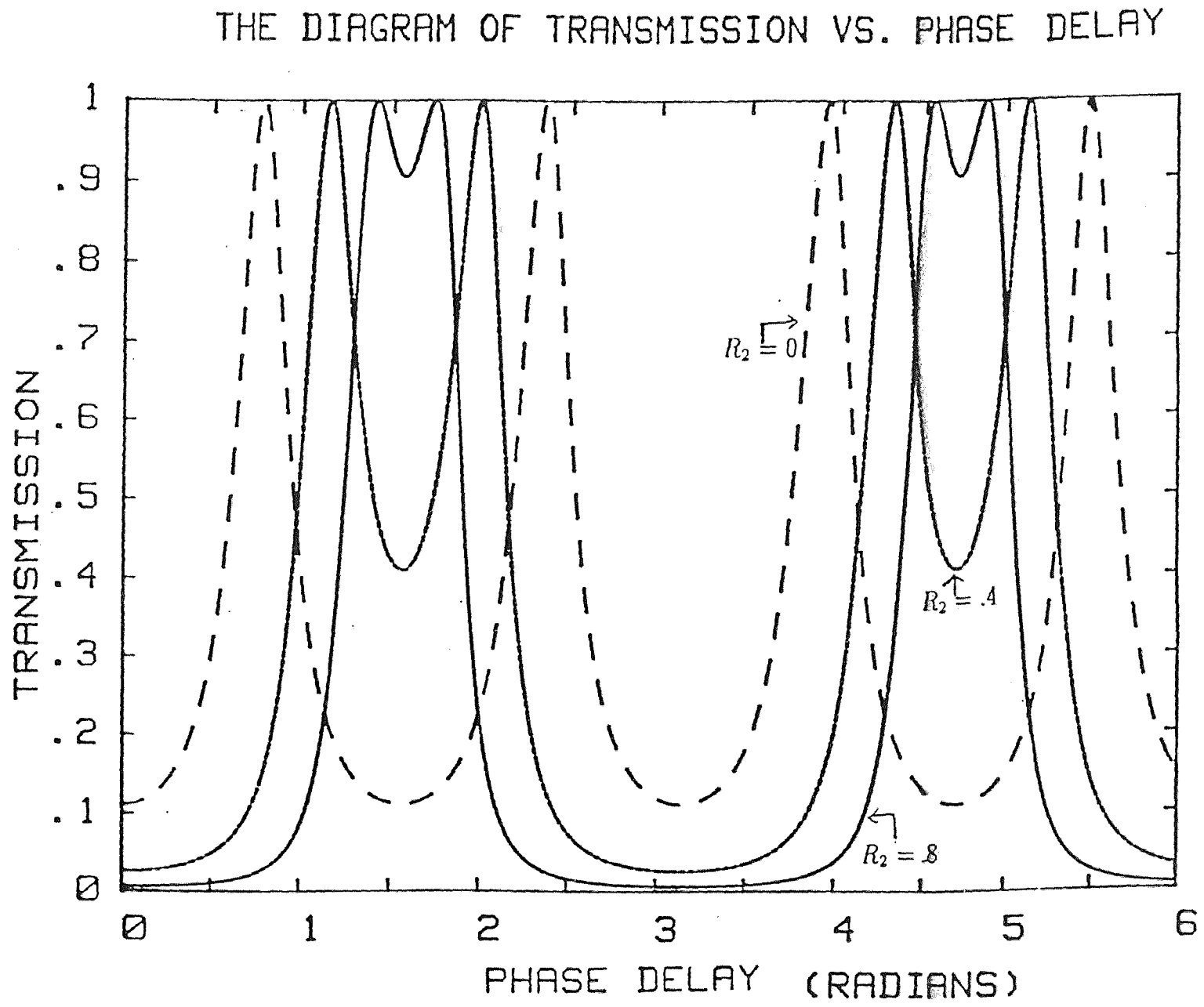

Figure 9a For three-interface Fabry-Perot etalon in the case of $r_{12} \leq 0$

$R_1 = R_3 = .5$, $\phi_1 = \phi_2$.

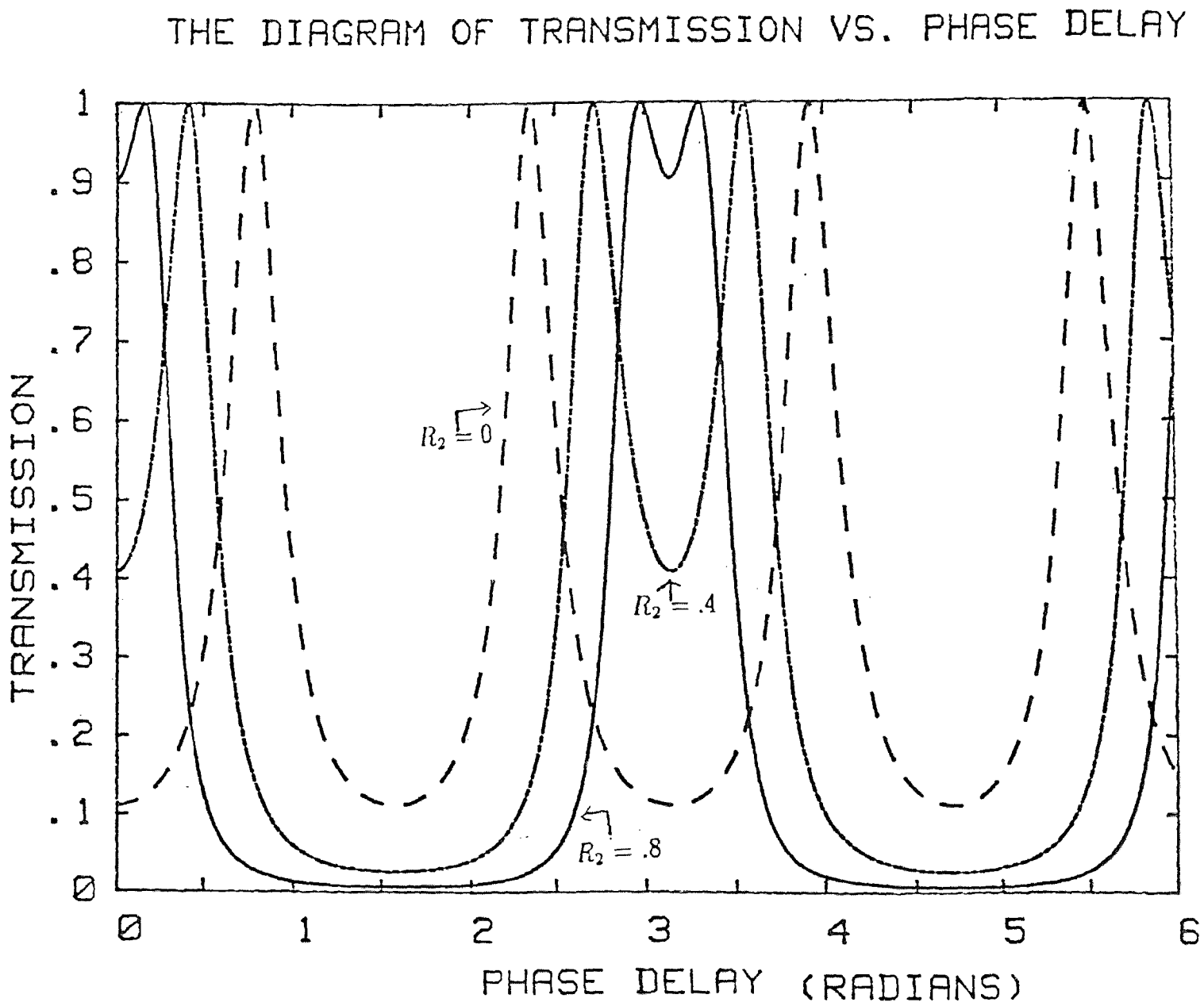

Figure 9b For three-interface Fabry-Perot etalon in the case of $r_{12} \geq 0$.

$R_1 = R_3 = .5$, $\phi_1 = \phi_2$.

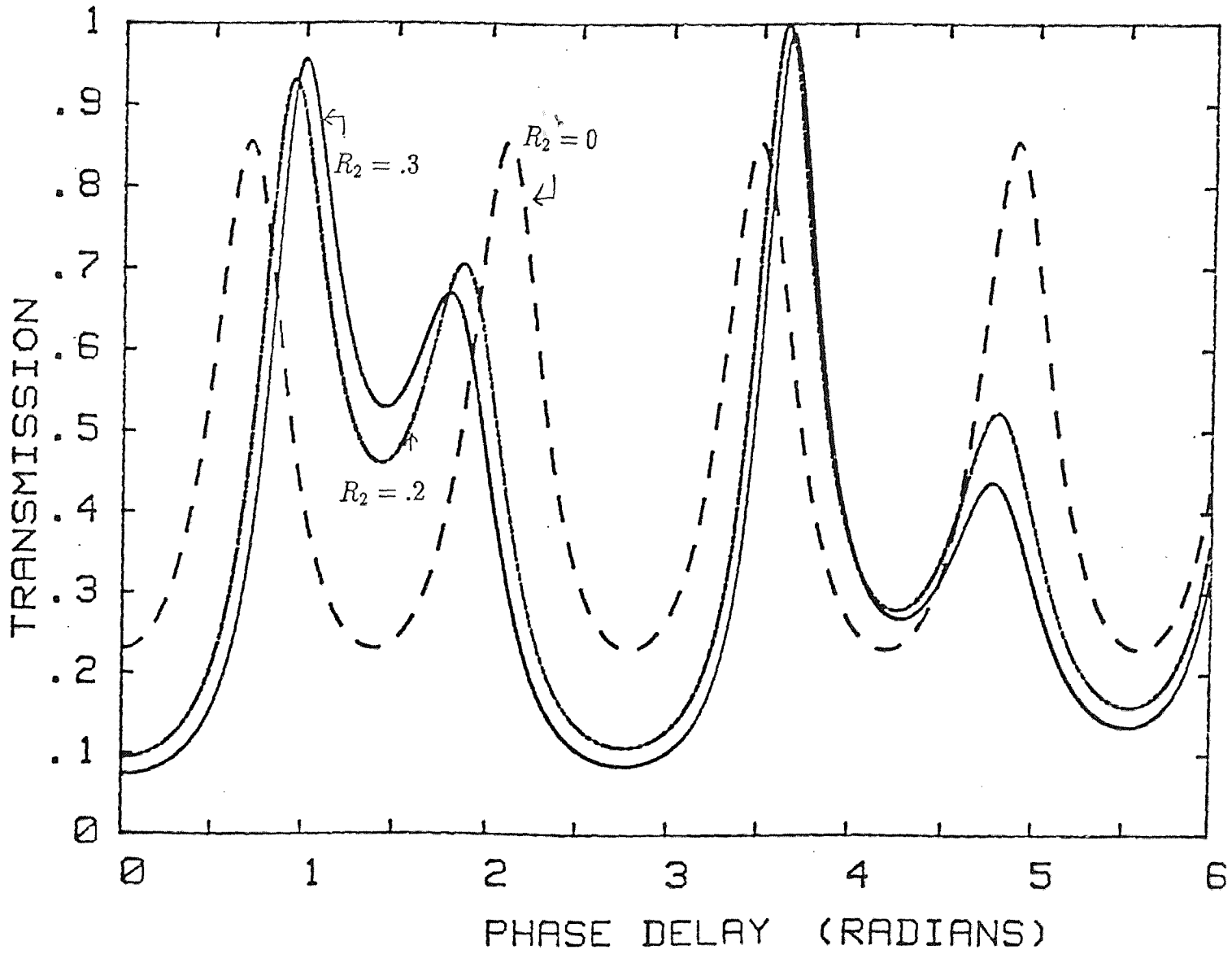

Figure 10a For three-interface Fabry-Perot etalon in the case of $r_{12} \leq 0$, $R_1 = .5$ $R_3 = .2$, $\phi_1/\phi_2 = 5/4$.

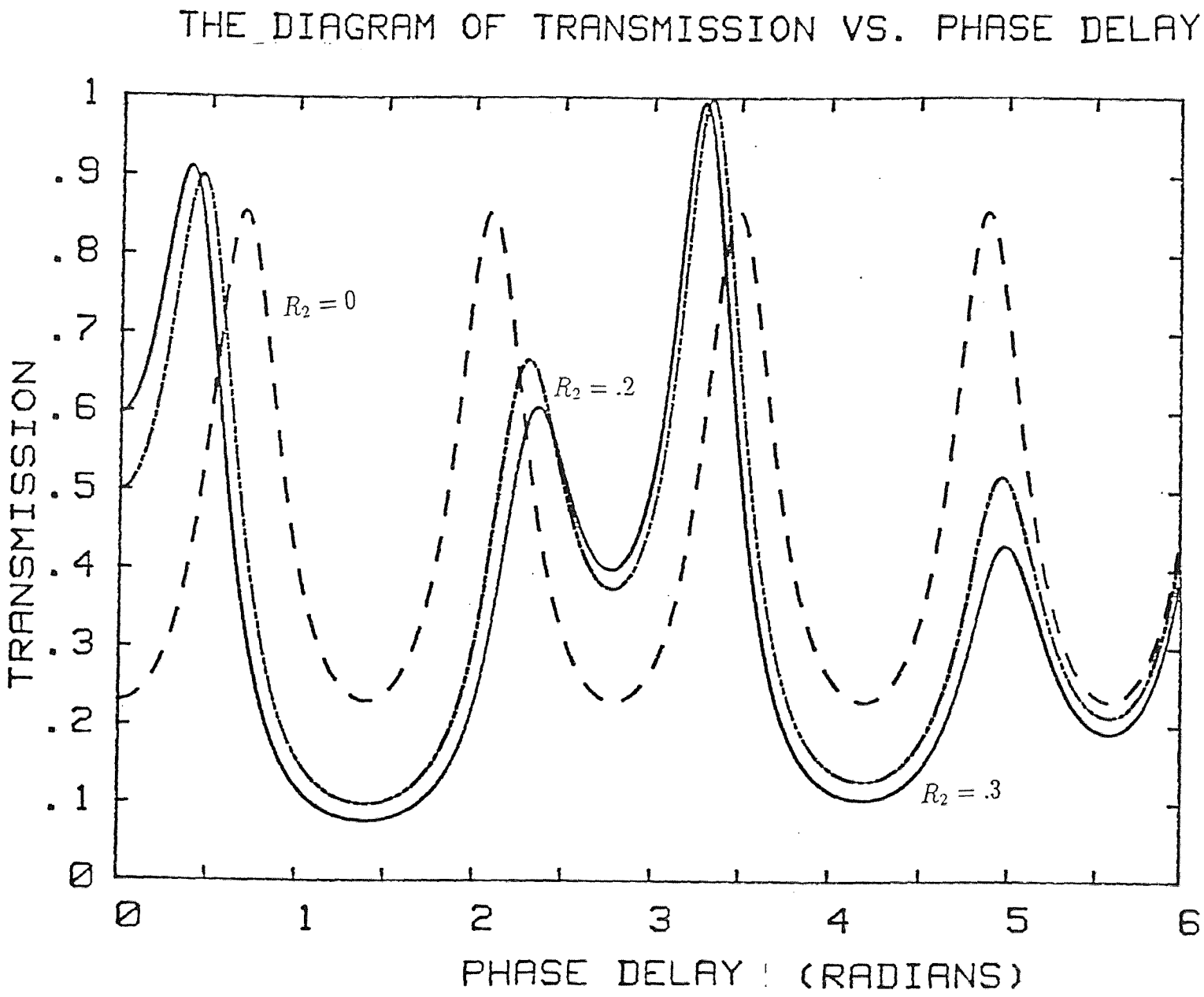

Figure 10b For three-interface Fabry-Perot etalon in the case of $r_{12} \geq 0$.
$R_1 = .5$ $R_3 = .2$, $\phi_1/\phi_2 = 5/4$.

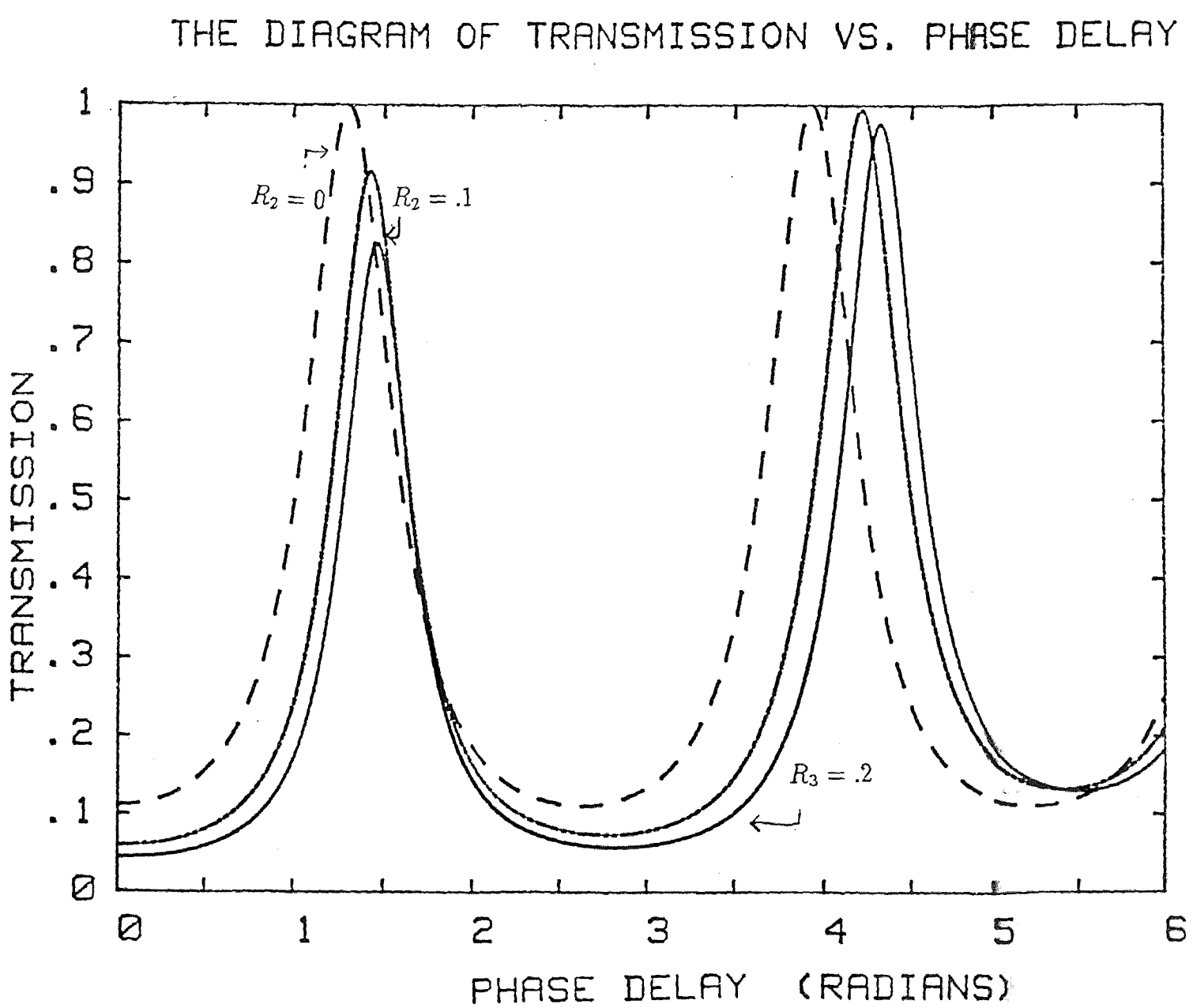

Figure 11a For three-interface Fabry-Perot etalon in the case of $r_{E2} \leq 0$. $R_1 = R_3 = .5$, $\phi_1/\phi_2 = 1/5$.

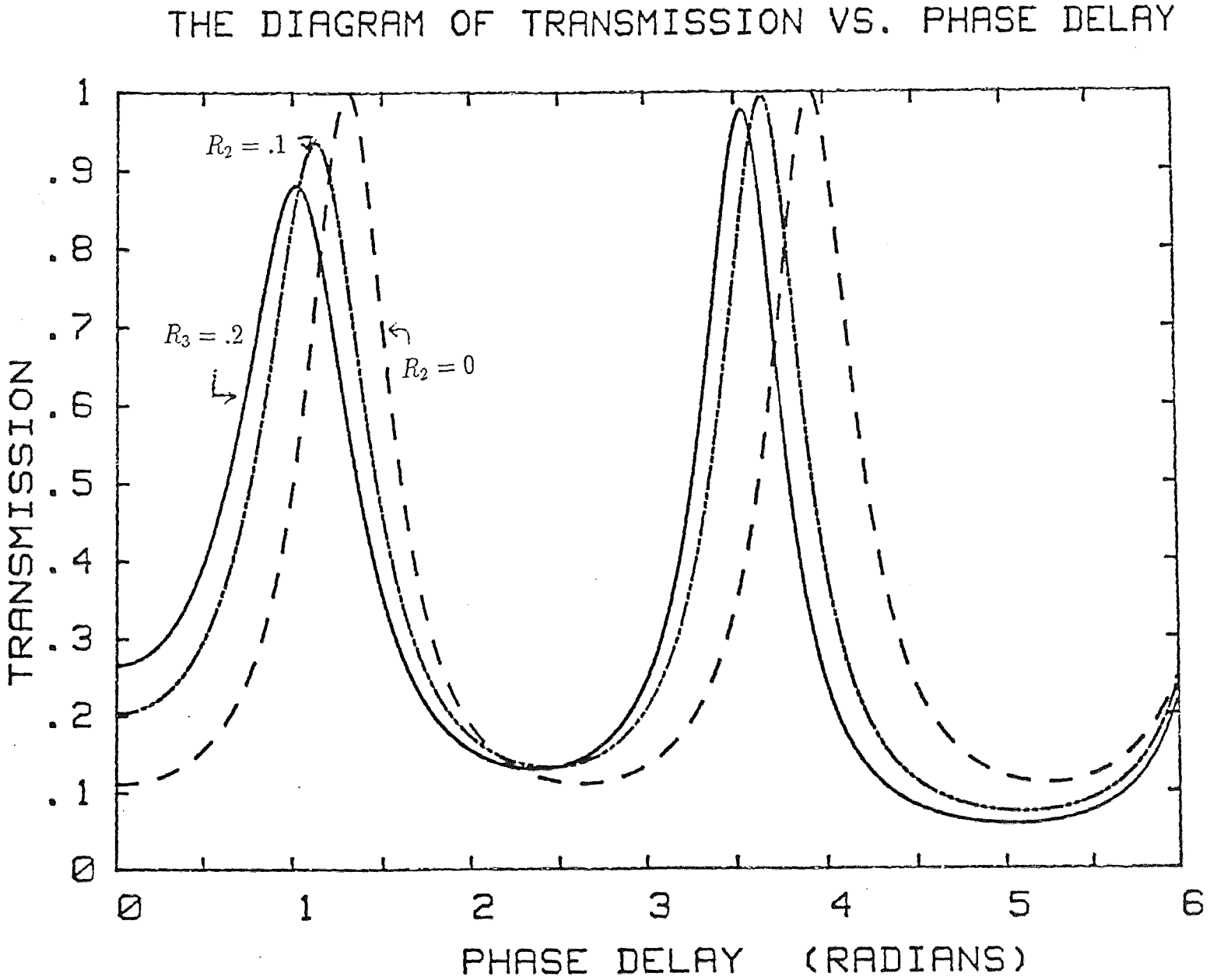

Figure 11b For three-interface Fabry-Perot etalon in the case of $r_{12} \geq 0$.

$R_1 = R_3 = .5,\ \phi_1/\phi_2 = 1/5.$

is very large , then an overall shift of the peaks' positions occurs without splitting as the reflectivity of middle interface is varied.

2.3 The Effect of Light Absorption on the Properties of Fabry-Perot Etalon

I. ABSORPTION IN THE REFLECTIVE SURFACES

At first, we consider a simple case - a two-mirror Fabry-Perot interferometer with the same mirror reflectivity. We can use the transmission expression of Eq. 11 :

$$\frac{I_t}{I_i} = \frac{T^2}{(1-R)^2 + 4Rsin^2(\frac{\delta}{2})}. \tag{11}$$

where $\delta = 4\pi nlcos\theta/\lambda$.

Rearranging Eq. 11 as

$$\frac{I_t}{I_i} = \frac{T^2}{(1-R)^2}\frac{1}{1+\frac{4R}{(1-R)^2}sin^2(\frac{\delta}{2})}. \tag{38}$$

R and T represent the reflectivity and transmission of mirrors.

Light absorption will be considered in the energy conservation relationship,

$$T + R + A = 1. \tag{39}$$

where A is the absorption of the reflective mirrors.

Substituting Eq. 39 into Eq. 38

$$\frac{I_t}{I_i} = (1 - \frac{A}{1-R})^2 \frac{1}{1 + \frac{4R}{(1-R)^2} sin^2(\delta/2)}. \tag{40}$$

Facter $[1 - \frac{A}{1-R}]^2$ can change the maxima of transmission. Figure 12 compares the effect of different absorption values A.

Let us consider the absorption of interfaces in three-mirror Fabry-Perot interferometer. Using the results of Eq. 31, Eq. 39, if the absorption is taken into account that Eq. 31 will become,

$$\begin{bmatrix} E_1^+ \\ E_2^- \end{bmatrix} = \frac{1}{t_1 t_2} \begin{bmatrix} e^{-i\phi_1} & -r_1 e^{+i\phi_1} \\ -r_1 e^{-i\phi_1} & (r_1^2 + t_1^2) e^{+i\phi_1} \end{bmatrix} \begin{bmatrix} e^{-i\phi_2} & -r_2 e^{+i\phi_2} \\ -r_2 e^{-i\phi_2} & (r_2^2 + t_2^2) e^{+i\phi_2} \end{bmatrix} \begin{bmatrix} E_3^+ \\ E_3^- \end{bmatrix} \tag{41}$$

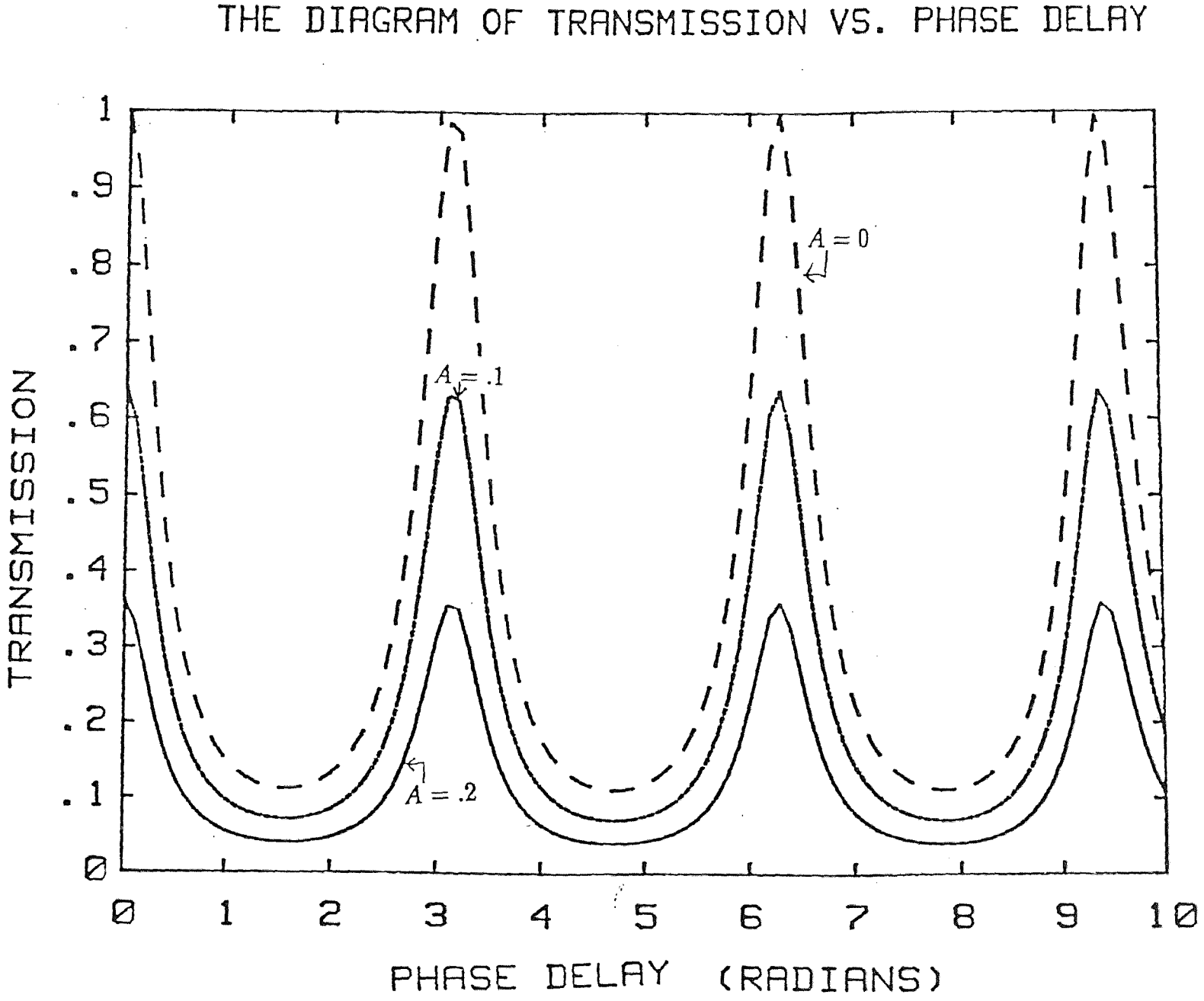

Figure 12 The result of Eq. 36 for different absorption factor A.

intensity transmission as:

$$\frac{I_t}{I_i} = \frac{(1-R_1-A_1)(1-R_2-A_2)(1-R_3-A_3)}{D_1}. \qquad (42)$$

A_1, A_2 and A_3 are the absorption at interfaces 1, 2 and 3 respectively and the denominator D_1 is as the follow,

$$D_1 = 1 + (r_1 r_2)^2 + (r_2 r_3)^2 + (r_1 r_3)^2(1-A_2)^2$$

$$+2r_1 r_2[1 + r_3^2(1-A_2)]cos2\phi_1 + 2r_2 r_3[1 + r_1^2(1-A_2)]cos2\phi_2$$

$$+2r_1 r_2^2 r_3 cos(2\phi_1 - 2\phi_2) + 2r_1 r_3(r_2^2 + t_2^2)cos(2\phi_1 + 2\phi_2). \qquad (43)$$

Figure 13 shows the effects of absorption in three-interface Fabry-Perot etalon for different A_2.

The absorption at the interfaces may be represented by the attenuation constant α, which can be derived from Maxwell's equations. [12]

$$\alpha \approx \sqrt{\frac{\omega\mu\sigma}{2}} \qquad [for\ conductor\ (\frac{\sigma}{\omega\mu})^2 >> 1]. \qquad (44)$$

where μ – permeability of medium, ω – the angular frequency of fields and σ – conductivity. μ, ω, σ and the thickness of the medium are the parameters of the

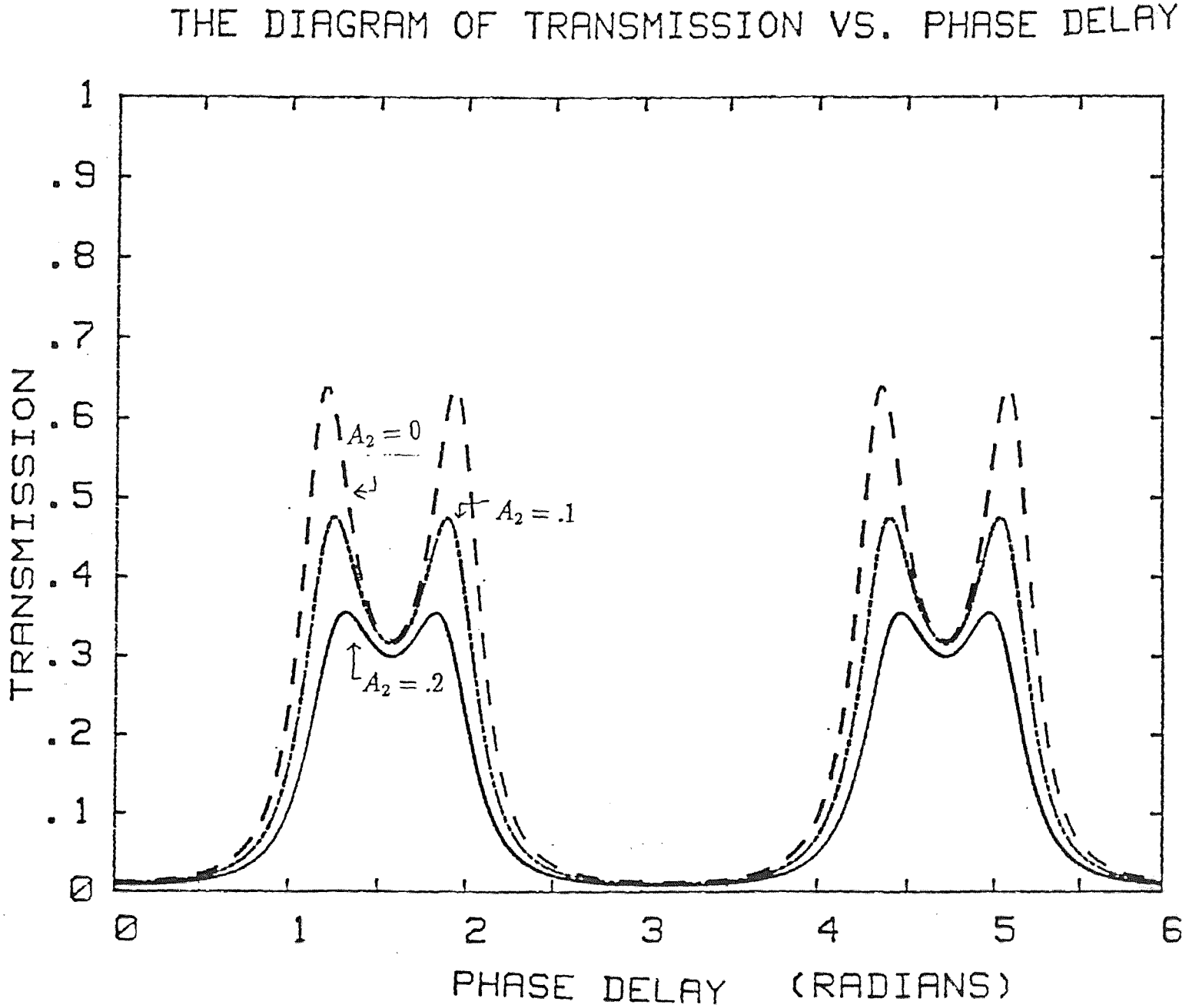

Figure 13 The result of Eq. 42 for different A_2

$A_1 = A_3 = .1, R_1 = R_2 = R_3 = .5, \sigma_1/\sigma_2 = 1$

light absorption of medium.

II. ABSORPTIONS IN THE SPACER LAYER

When the absorption in the spacer layer is taken into account, Eq. 6 is modified as

$$A_t = tt'e^{-\frac{k}{2}}A + tt'e^{-\frac{3k}{2}}r^2e^{i\delta}A + tt'e^{-\frac{5k}{2}}r^4e^{2i\delta}A + \cdots + \ldots \quad (45)$$

where $e^{-\frac{k}{2}}$ is the attenuation in the wave amplitude for each pass through the material. Neglecting the absorption in the interfaces, we set $tt' = 1 - R$ and, thus, Eq. 45 becomes,

$$\begin{aligned} A_t &= (1-R)e^{-\frac{k}{2}}[1 + Re^{-k}e^{i\delta} + R^2e^{-2k}e^{2i\delta} + \ldots]A \\ &= \frac{(1-R)e^{-\frac{k}{2}}}{1 - Re^{-k}e^{i\delta}}. \end{aligned} \quad (46)$$

The transmission $T = \frac{A_t^2}{A^2}$ of the intensity is,

$$T = \frac{(1-R)^2 e^{-k}}{1 + 2R^2 e^{-2k} - 2Re^{-k} cos\delta}$$
$$= \frac{(1-R)^2 e^{-k}}{(1-Re^{-k})^2} \frac{1}{1 + \frac{4Re^{-k} sin^2(\delta/2)}{(1-Re^{-k})^2}}. \qquad m(47)$$

If R is replaced by $R' = Re^{-k}$, Eq. 45 can be writen as :

$$T = \frac{(1-R)^2 e^{-k}}{(1-Re^{-k})^2} [\frac{1}{1 + \frac{4R' sin^2(\delta/2)}{(1-R')^2}}]. \qquad (48)$$

The factor in the square brackets is the same as the expression in Eq. 11 with the modification of an effective reflectivity $R' = Re^{-k}$, and an overall attenuation factor, given by $\frac{(1-R)^2 e^{-k}}{(1-Re^{-k})^2}$.

When comparing Eq. 40 and Eq. 47 , the absorption caused by the metallic coating only changes the maximum value of the transmission profile. On the other hand the absorption due to the spacer layer decreases the reflection coefficient by the amount $R' = Re^{-k}$.

III. THE ABSORPTION OF SPACER AND MIRRORS

The general transmission expression involving absorption in the metallic coating

and in the spacer layer ofr two-mirror Fabry-Perot etalon is, therefore, given by:

$$T = \frac{(1-R-A)^2 e^{-k}}{(1-Re^{-k})^2} \frac{1}{1+\frac{4R'sin^2(\delta/2)}{(1-R')^2}}. \tag{49}$$

In the case of three-interface Fabry-Perot etalon, if the absorption of spacer and interfaces are taken into account that Eq. 31 will become,

$$\begin{bmatrix} E_1^+ \\ E_1^- \end{bmatrix} = \frac{1}{t_1 t_2} \begin{bmatrix} e^{-i\phi_1} e^{-\frac{k_1}{2}} & -r_1 e^{+\phi_1} e^{-\frac{k_1}{2}} \\ -r_1 e^{-i\phi_1} e^{-\frac{k_1}{2}} & (r_1^2+t_1^2) e^{+i\phi_1} e^{-\frac{k_1}{2}} \end{bmatrix}$$
$$\begin{bmatrix} e^{-\phi_2} e^{-\frac{k_2}{2}} & -r_2 e^{+i\phi_2} e^{-\frac{k_2}{2}} \\ -r_2 e^{-i\phi_2} e^{-\frac{k_2}{2}} & (r_2^2+t_2^2) e^{+i\phi_2} e^{-\frac{k_2}{2}} \end{bmatrix} \begin{bmatrix} E_3^+ \\ E_3^- \end{bmatrix}. \tag{50}$$

where $e^{-\frac{k_1}{2}}$ and $e^{-\frac{k_2}{2}}$ are the attenuation in the wave amplitude for each pass through the spacer 1 and 2 respectively. The intensity transmission is,

$$T = \frac{(1-R_1-A_1)(1-R_2-A_2)(1-R_3-A_3)}{D_2}. \tag{51}$$

We can derive D_2 as,

$$D_2 = e^{-(k_1+k_2)} D_1. \tag{52}$$

here D_1 is Eq. 43.

A graph of Eq. 51 is given in Figure 14.

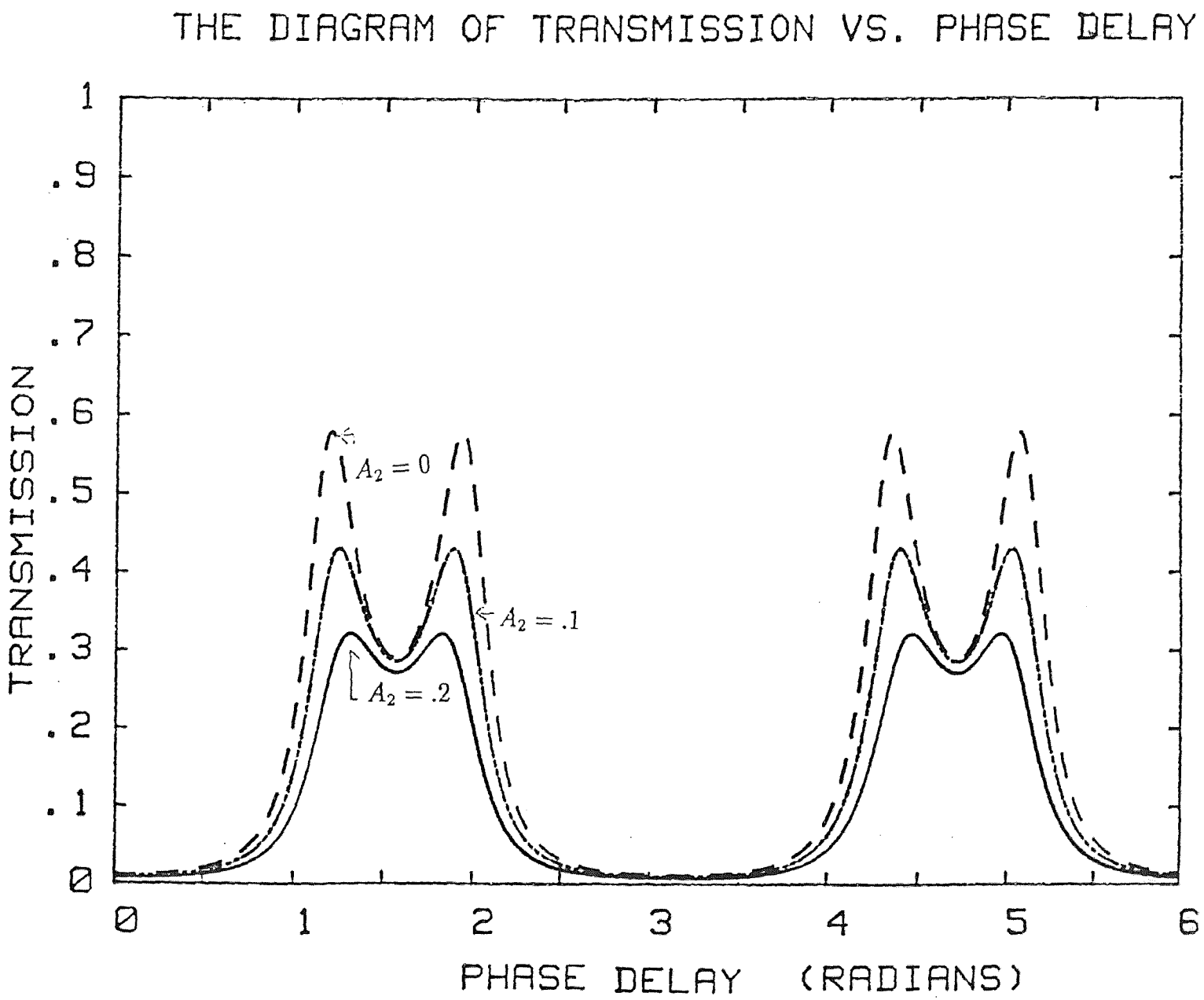

Figure 14 The result of Eq. 51 for different A_2

$A_1 = A_3 = .1, R_1 = R_2 = R_3 = .5, \phi_1/\phi_2 = 1$

The purpose of the experiment is to observe photo-induced effect on the photo-sensitive material, CdS thin layer, under the illumination of other light source and to obtain the change of refractive index.

From Figures 9a or 9b we can see that the splitted peaks will get closer as reflection of the middle interface becomes larger. So we can use the position change of the splitted peaks to derive the reflection of the middle interface, that is, use the equal relationship of Eqs. 33 between the conditions of with and without the influence of the other photonic sources. The change of reflection represents that the index of refraction has been changed too (see Eq. 30), so we can derive the change of index of refraction from the following equation (assuming the light is incident from medium 1 to mudium 2 and their indices of refraction are n_1 and n_2 respectively),

$$\frac{\triangle R}{R} = \frac{4n_1 \triangle n_2}{n_2^2 - n_1^2}. \tag{54}$$

In this experiment, R is the reflectiivity of CdS thin layer in dark room, $\triangle R$ and $\triangle n$ are the changes of the reflectivity and refractive index of the Conditional Artificial Dielectric CdS thin layer.

3 Deposition of Thin Films

For fabricating a Fabry-Perot etalon we used two different film deposition techniques, one is plasma polymerization of PMMA and the other is vacuun evaporation deposition of CdS and aluminum. In this chapter, we introduce the principle of thin film deposition and describe the apparatus.

3.1 Principle of Thin Film Deposition

I. POLYMER DEPOSITION

Methyl methacrylate monomer was used as a starting material in the plasma deposition process. The methacrylate acid is a clear, colorless liquid a pleasant ethereal odor that reacts with numerous reagents and polymerized rapidly. Polymethyl methacrylates are tough thermo-plastic solids, which are characterized by their transparency, dimensional stability, lightness, and resistance to weather and chemicals. Table 1 list the physical properties of methyl methacrylate

BOILING POINT	$\simeq 100°C$
INDEX OF REFLECTION	$n \simeq 1.415$
VAPOR PRESSURE	$\simeq 35mmHg(at20°C)$ $\simeq 53mmHg(at30°C)$
HEAT OF POLYMERIZATION	$\simeq 11.6Kcal/mol$

Polymers are defined as the high-molecular-weight inter-reaction products of related polyfunctional molecules, and the process by which polymers are obtained is called polymerization. Polymerization reactions are the chemical reactions responsible for combining the polyfunctional molecules into polymers. Plasma polymerization is one of the methods of polymerization reaction.

In this technique the vapor of monomer are polymerized by ionization of the monomer molecules. Some ionization of the monomer molecules is enough to start a chain reaction and a polymeric film is deposited on the substrate. Deposition may be achieved on many kinds of substrates [24]. Ionization was achieved in our experiments by a simple two electrode structure, with spacing of 3 cm, and a voltage drop of about 600 volts. The deposition is sensitive to the pressure at which chain reaction takes place. Thus most of this reactions are made in

a vacuum chamber where pressure of the monomer vapor is carefully controlled. Moreover thermal effects may change the composition and thus density and the rate of the reaction. Some systems use gas carriers to deliver the monomer vapours into the vacuum chamber. This have been shown to have benificial effect on the quality of film deposited and the rate of deposition. [8] Other method of discharge, such as, rf discharge has been tried too. [7] RF discharge has the advantage of uniform ionization method on the expense of relatively slow deposition rate. DC discharge was found to be inefficient and produces a low quality films. AC discharge was found to be of highest deposition rate with moderate film quality. In our Laboratory we use the latter technique for its simplicity and speed.

II. VACUUM DEPOSITION

Vacuum deposition is used to make the thin films of Al and CdS. In vacuum both metals and thermally stable compounds begin to evaporate rapidly when their temperature has been sufficiently raised for their vapor pressure to have reached a value in excess of 10 microns Hg. Under conditions of high vacuum and where the vapor pressure of the substance if less than about 1 mmHg, the vapor molecules

can be assumed to leave the emitting surface relatively unimpeded. The mass of substance removed as vapor from unit area and in unit time at a given temperature will be the same as that evaporating from the surface of the substant in equilibrium with its saturated vapor. For equilibrium the rate at which molecules evaporate must be equal to the rate at which they condense on the emitting surface. The number of molecules impinging on unit area in unit time is given by the relation $\frac{1}{4}nv$ where n is the numger of molecules per unit volume and v is their average velcity. If only a fraction a of the molecules arriving at the surface are condensed, then for equilibrium the number of molecules evaporating from unit time will be $\frac{1}{4}an$. Then the rate of evaporation in vacuum is [24]:

$$5.85 \times 10^{-5} \times a \times P_{\mu} \times \sqrt{\frac{M}{T}} \qquad g\ cm^{-2}\ sec^{-1}$$

where P_{μ} is the vapor pressure in microns Hg at T°K and M a mol of the substance being evaporated.

3.2 The Apparatus of Thin Film Deposition

I. VACUUM EVAPORATOR

The system used for fabricating CdS and Al thin film consists of four three sections – vacuum chamber, pumping system, vacuum gauges and evaporation source with electrical controls and filament supply. We will describe these sections separately . (see Figure 15)

- Vacuum chamber consists of a Pyrex bell jar and gasket resting on a stainless steel baseplate. A cylinder welded underneath the boreplate contains the main valve and an LN2 baffle. The bottom of the cylinder is a plate to which the diffusion pump is bolted. There are two vacuum pumps – a high speed oil diffusion pump and mechanical pump. The mechanical pump bring the chamber pressure down to $\sim$ 20 mtorr, but the diffusion pump can pump the system go down to $\sim 10^{-6}$ in a short time. The diffusion pump can work only under a low pressure, i.e. $\leq$ 50 mtorr. Before the heater of the diffusion pump is turned on the pressure in the system has to be below 50 mtorr.

- The vacuum gauging includes two Hastings thermocouple gauges. The thermocouple gauge controller has a selector switch to read pressures down to one millitorr at the mechanical pump (TC-1) or in the bell jar (TC-2). An ionization guage with a controller can read the pressure above the diffusion

pump in the range 10^{-4} to 10^{-6}.

- On the hinged control panel, there are main switch, a circuit breaker, and switches to turn on the mechanical pump, the diffusion pump, and the filament power supply, filament glow selector and the rotary fixture. The current passing through the electrodes is measured by the 0 – 50 amp ammeter on the instrument panel. The variable transformer ranges from 0 to 100 percent of full scale to give 0 to 24 volts. We used a tungsten wire on which Al wire was hung as a filament source for deposition. We used a ceramic basket to hold the CdS powder. Around the basket a wounded tungsten wire was used as a heater.

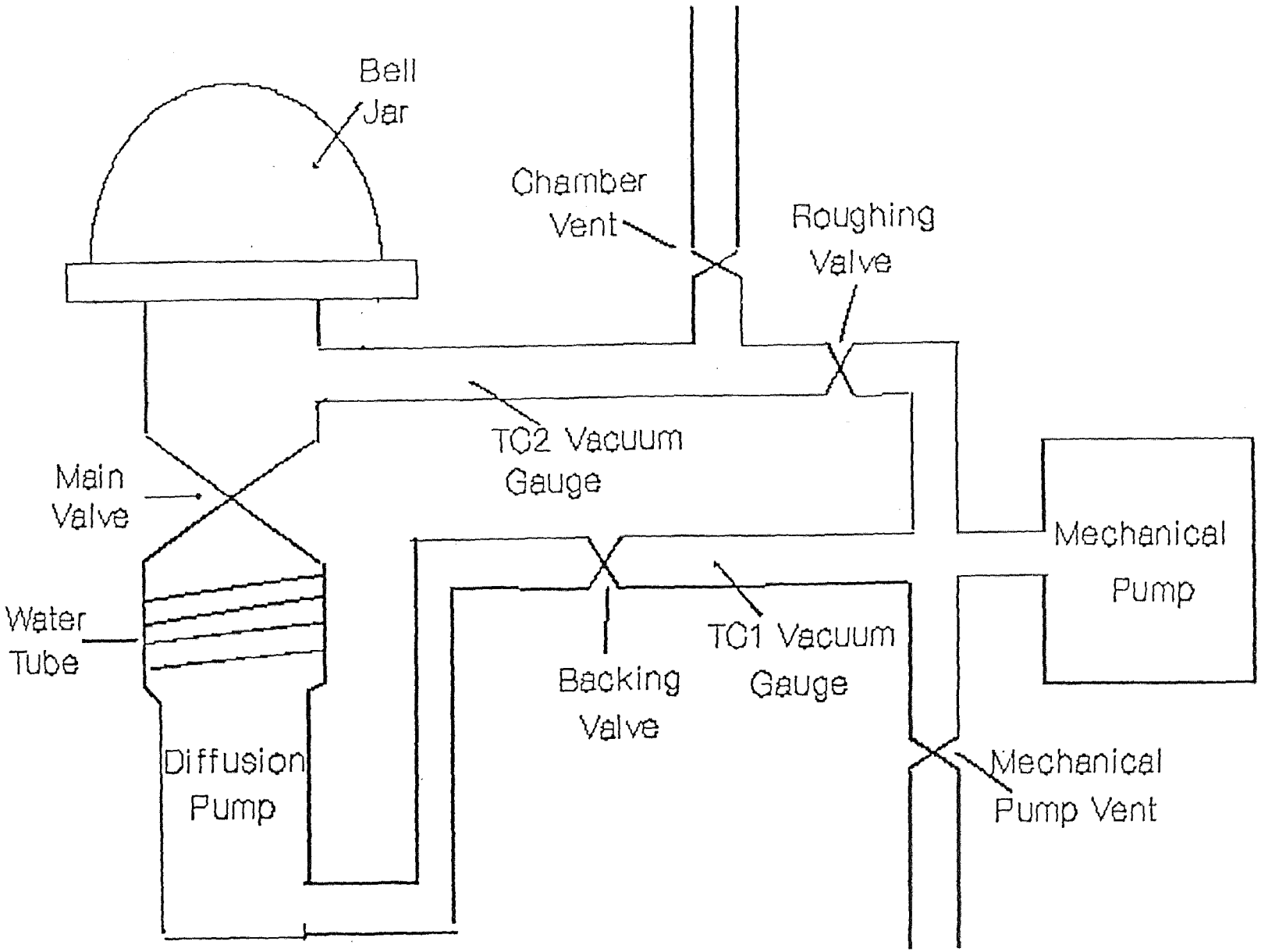

Figure 15 The structure of vacuum evaporator.

II. PLASMA GENERATOR

The system consists of the vacuum chamber is made of cross shaped Pyrex, mechanical pump, diffusion pump, valves, vents and electrical power connected to the system.

In Figure 16 we can see the system more clearly. The electrical power is connected between two electrode plates. The top plate has been drilled many holes which will let the vapor of monomer go through and be deposited on the substrate uniformly. The dimension of the plates are $2.5 \times 7.5 \times 0.1\ cm^3$. They are made of stainless steel and are separated from one another by a distance of 3 cm. The substrates, usually glass slides or microscope cover glass, are layed on the bottom plate. A voltage is then applied to the electrodes and a dischange glow, of deep blue, is induced. The color of the discharge and its distribution around the electrodes is characteristics to the applied voltage and the vacuum pressure [25]

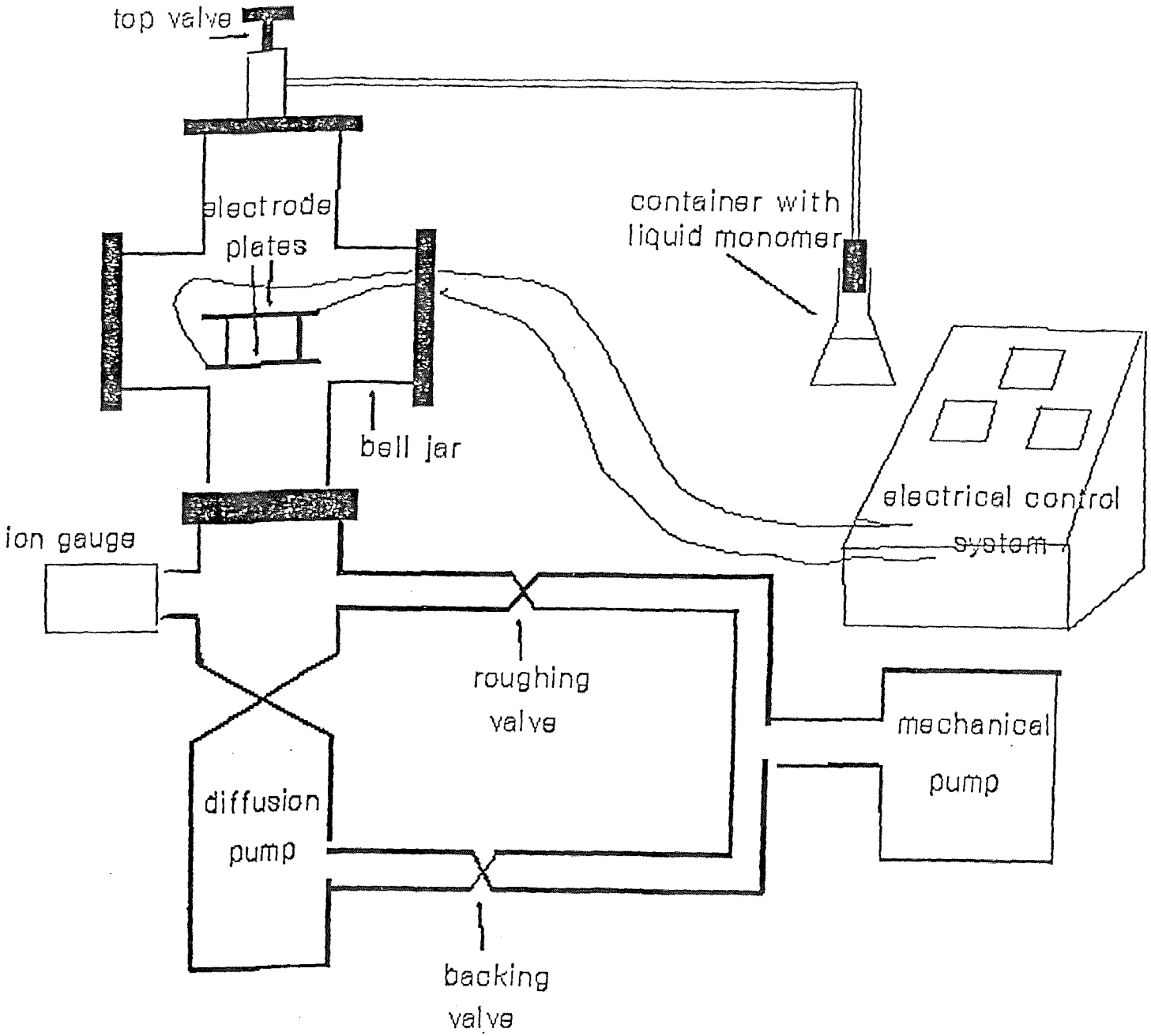

Figure 16 The structure of plasma generator.

4 Experiment and Results

4.1 Fabry-Perot Etalon Fabrication

I. NECESSARY MATERIAL

1. Cover glass substrate (size : 22 mm x 22 mm square)

2. Micro-slide glass

3. Pure aluminum wire for evaporation deposition

4. Liquid methyl mehtacrylate monomer for plasma polymerization

5. Cadmium sulfide powder

6. Methonal, aceton and distilled water for cleaning glass substrate

II. PROCEDURE OF FABRICATION

CLEANING GLASS SUBSTRATES

1. Put the cover glass substrate and micro-slide glass into beaker which contains distilled water and detergent.

2. Put the beaker into ultrasonic bath for 15 minutes.

3. Rinse these glasses with water until wash away the detergent and then soak thses glasses into aceton and methonal.

4. Take these glasses out and dry them in oven. Now these glasses are ready to be used.

5. Stick the cover glass substrates on micro-slide with tape.

CASE I ALUMINUM AND CdS THIN FILM DEPOSITION

1. Soak the aluminum wire into the aceton to wash away foreign material on the surface of wire.

2. Turn on the mechanical pump, open the backing valve and choose the thermocouple TC1. Turn on the diffusion pump heater as the the reading of TC1 is around 50 mtorr.

3. Put the micro-slide with cover glass into the chamber and the distance between the evaporating source and glass is about 20 cm (Notice: the distance should not be too close that will burn the polymer layer and form the milky

Al thin film). Take the aluminum from aceton and hook the aluminum wire on the tungsten wire. Let aluminum be evaporated upward to the galss substrate.

4. Close the backing valve. Put down the bell jar in proper position and then open the roughing valve to pump the chamber to 50 mtorr (now the thermocouple gauge selector switch is at TC2). Close the roughing valve, open the backing and main valves. Pump the chamber for 30 minutes (for better vacuum condition).

5. After the pressure in the chamber goes down to $\sim 10^{-5}$ torr, turn on the filament power (the current flow through the filament is about 34 amps.). As soon as the aluminum has melted open the shutter , above the source, for 15 seconds (Al thin film) or for 3 mins (CdS thin film).

6. Close the shutter and turn off the filament power and the heater of the diffusion pump. Close the main valve, but keep the backing valve open and mechanical pump on until the diffusion pump cools down. Wait about 30 minutes, take out the glass substrates.

CASE II PLASMA DEPOSITION

1. Put the substrate on the bottom electrode in the vacuum chamber.

2. Keep the top valve of the chamber open and pump the system. The procedure of pumping the system is the same as that of the evaporation deposition. When the vacuum condition of the chamber is about 10^{-5} torr, let some monomer flow into the chamber to purify the chamber.

3. Then turn off the diffusion pump, close all valves (except the top valve) and let the monomer vapor fill the chamber (the pressure should be greater than 100 mtorr). After the chamber has been filled with monomer vapors open the valve to the mechenical pump. This procedure will ensure proper stream away from the chamber and will not suck air through the mechanical pump owing to negative pressure.

4. Open the roughing valve, adjust the pressure of the chamber to 300 mtorr (this pressure will influence the rate of deposition) and tuen on the power supply. Adjust the voltage across the electrode is around 550 V (AC voltmeter) for 1.5 hour.

5. After the deposition, close the roughing valve and open the backing valve until the diffusion pump cools down. Wait about 20 minutes to cool down the substrates and remove them.

4.2 The Structure of Samples

In Figure 17 we show the structure of the samples used in our experiments. Samples (i) and (iii) are regular Fabry-Perot etalons without any artificial dielectric layer while sample (ii) and (iv) include this layer. Sample (v) and (vi) are three-mirror Fabry-Perot etalon.

The description of the sample structure is as follows :

- Sample (i) – a regular Fabry-Perot etalon with a spacer layer comprises of two glass layers and a polymeric layer. The mirrors are partially reflecting Al films.

- Sample (ii) – similar to sample (i) with the inclusion of Conditional Artificial Dielectrics layer (CdS embedded clusters layer) at the interface of a polymeric layer and glass.

- Sample (iii) – a regular Fabry-Perot etalon with a spacer of one polymeric layer.

- Sample (iv) – similar to sample (iii) but with the inclusion of Cconditional Artificial Dielectric layer (CdS embedded cluster layer) in the middle of the spacer layer.

- Sample (v) – A ragular etalon with three mirrors separately by polymeric layer and two glass layers.

- Sample (vi) – similar to in sample (v) with the substitution of the glass layers with polymeric alyers.

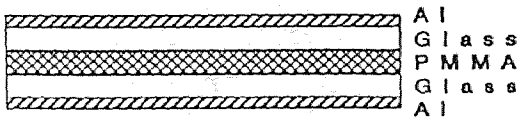

(i)

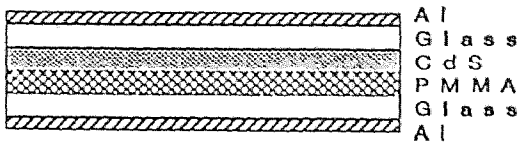

(ii)

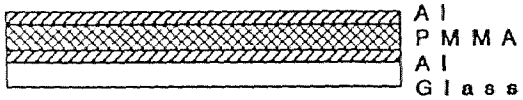

(iii)

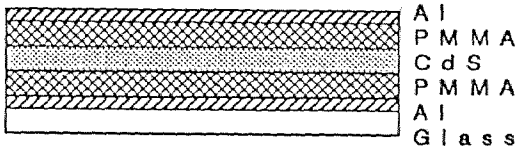

(iv)

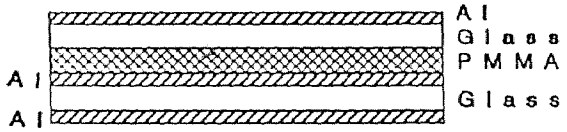

(v)

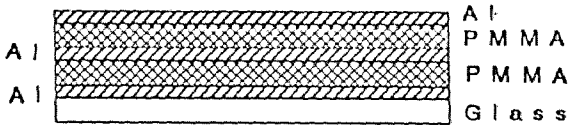

(vi)

Figure 17 The structure of samples in this experiment.

4.3 Optical Measurement

I. MEASURING THE TRANSMISSION THROUGH A FABRY-PEROT ETALON

A. COMPONENTS

Figure 18 shows the components and the transmission measurement configuration. The components are described separately below.

1. Laser – We choose a He-Ne laser (wavelenght $\lambda = 0.6328 \mu m$) , because its photon energy is below the bandgap of pure CdS material which is 2.42 eV and the corresponding absorption wavelenght is between 450 to 500 nm.

2. Polarizer – In this experiment we would like to see the difference between transmsission of TE and TM modes.

3. Chopper – The chopper is connected to the Lock-in amplifier to provide a known modulating frequency.

4. Lens – The function of the lens is to diverge the laser light spot and increase the resolution.

5. Sample – The sample is mounted on a rotatable stand which controls the incident angles of laser light.

6. Filter – Only red light ($\lambda = 6328 \pm 5\mathring{A}$) can pass through the filter.

7. Detector – The detector which is connected to Lock-in amplifier detects the transmitted light through the Fabry-Perot etalon.

8. Lock-in amplifier – The reference frequency and input signal are provided from the chopper and the detector respectively. The Lock-in amplifier analyzes the input signal at a reference frequency to increase the signal-to-noise ratio.

9. White light source or "blue" laser – These light sources aims at the sample for stimulating the electrons from valence band to conducting band.

10. HP-300 Computer – The computer can read the data from Lock-in amplifier and save them.

11. Plotter – Connected to computer.

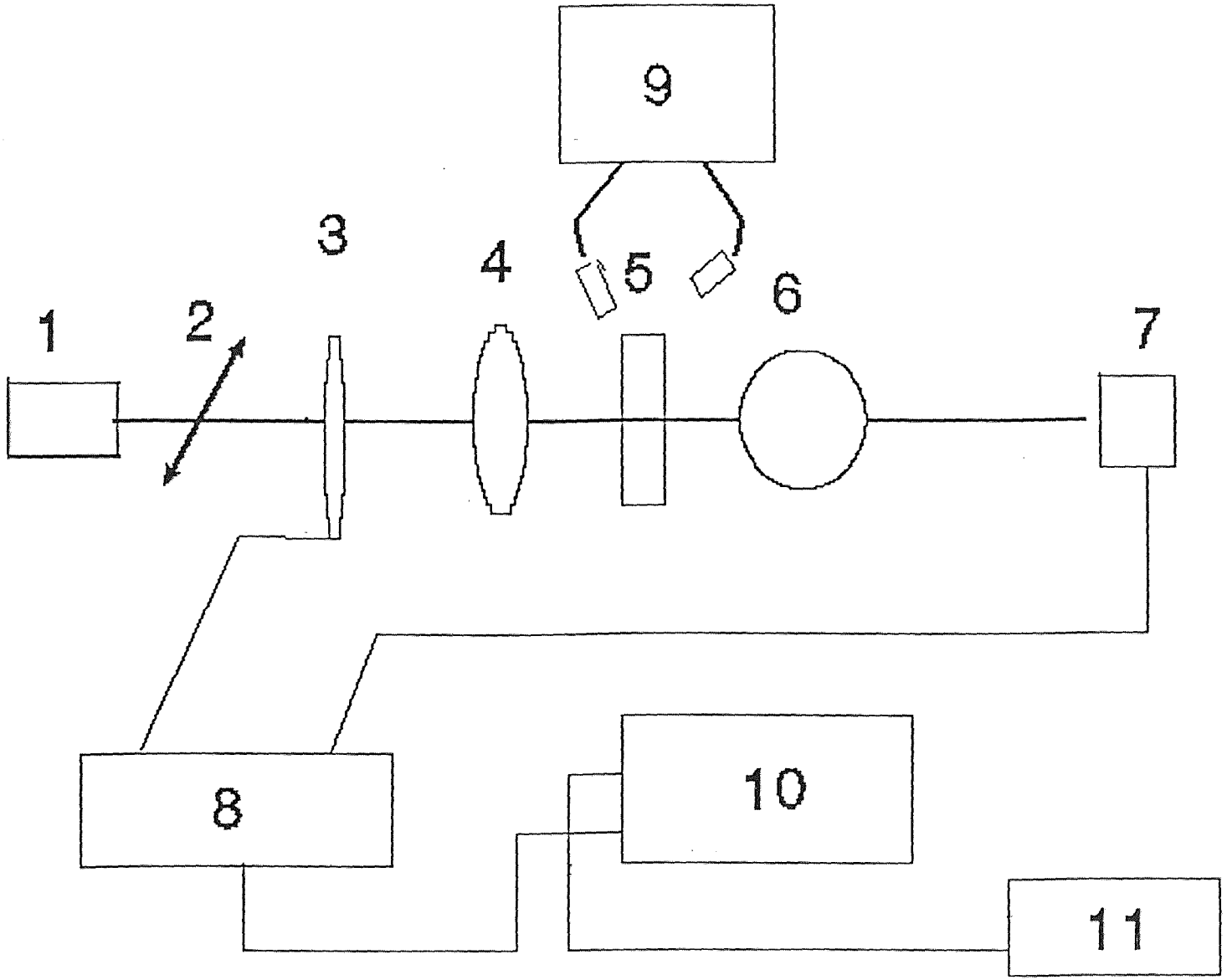

Figure 18 The measuring setup for transmission

B. EQUIPMENT SETUP

The first step is to find the normal incident angle to the sample and make sure that it is symmetrical with respect to rotating the sample in each direction. Set the normal angle to zero degree. Modifying the phase shift between the reference frequency and input signal to the Lock-in amplifier to maximize the signal reading. A pin-hole in front of the detector in placed to let only collimated rays to be measured.

Rotate the sample stand slowly, observe the reading shown on the Lock-in amplifier and then decide the interesting range of incident angles. Usually, we choose the small incident angle range ($\leq 10°$), because the larger incident angle range will result in a closer distance between two neighboring peaks as, thus, a limited resolution.

C. MEASUREMENT PROCESURE

1. Set the rotatable stand to the starting angle.

2. Adjust the frequency of the chopper and the phase shift , time constant of Lock-in amplifier.

3. Set the starting, ending and increment degree for controlling the computer to read the data from Lock-in amplifier.

4. Start to measure the transmitted intensity and wait the "BEEP" from computer to change incident angle. The duration must be long enough to stablize the reading.

5. Save the data when the measurement has done and plot the results.

II MEASURING OF THICKNESS OF PMMA

The purpose of this measurement is to measure the thickness of the polymer (PMMA) on the substrate. The magnified image of the polymer film is impinging on a screen. The film thickness is then calculated from the image dimension for the known magnification factor.

The components and arrangement are as shown in Figure 19 .

1. Laser – He-Ne laser, $\lambda = 0.6328\mu m$, output power is about 1mW.

2. Microscope objective 1 – ×20 put on adjustable stand focus the laser beam on the surface of the waveguide sample.

3. Waveguide sample – PMMA on micro-slide glass.

4. Microscope objective 2 – To magnify the near field pattern of the waveguide.

5. Screen – Let the laser project on the screen and measure the thickness of waveguide on the screen.

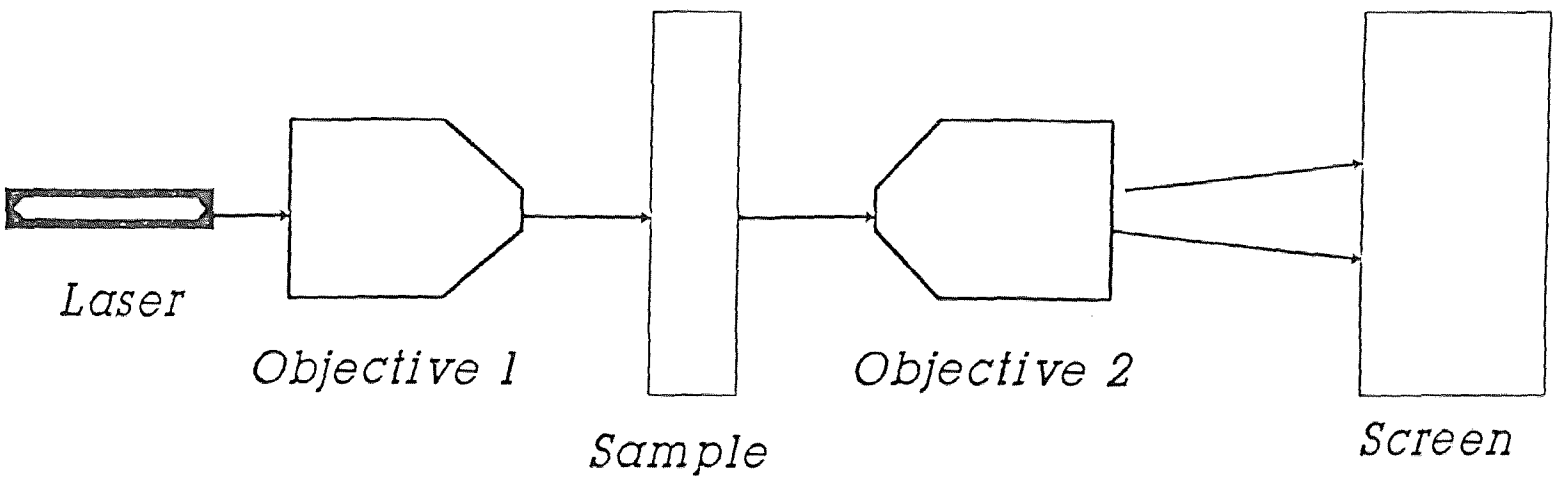

Figure 19 The measuring setup for thickness of PMMA.

4.4 Experimental Results

A regular Fabry-Perot etalon is form by a PMMA layer as the spacer layer between two partially transmitting Al thin films on a glass substrate. In Figure 20 we show the transmission profile as a function of the incident angle θ'. From this figure we can calculate the thickness of the spacer layer from Eq. 13. The expression for $cos\theta$ was calculated from Snell's law using our experimental incident angle. By varying the incident angle one may vary the values of phase delay δ.

The sample configuration is Sample (i). The solid curve in Figure 20 was obtained in dark room condition while the dash curve was obtained while shining white light source on the sample. A shift of the transmission pattern was obtained even in the absence of A Conditional Artificial Dielectric layer signifying a possible heat effect.

In Figure 21 we show the result for the sample structure (ii). As theoretically predicted this structure may be treated as a three-interface Fabry-Perot. The device is also measured in dark room (solid curve) and under illumination of a "blue" laser (He-Cd laser $\lambda = .442\mu m$) on the sample (dash curve). We can observe easily that the effect of the "blue" laser is to change the transmission

profile through the device.

If the incident angles have been transfer to phase length (using Eq. 1 , the l can be derived from the peaks' positions in Figure 21, using Eq. 13), then we can redraw the relation between the transmission and phase length in Figure 22. The profile of the transmission looks almost the same as that of Fig. 21, due to the small range of θ' used.

In Figures 23 and 24 we show the result for another sample structure (ii). The structure can be treated a three-interface Fabry-Perot etalon. The reflectivities of interfaces 1 and 2 are not identical, being .2 and .5 repectively. Fig. 21 is the result for a H mode of polarization and Fig. 22 is the result for a E mode. The solid curve in figures 21 and 22 was obtained in dark room and the dash curve was obtained while shining white light source.

Figures 25 and 26 show the relation between the transmission and the optical phase length (phase delay)which using the data of Fig. 23 and 24 respectively. Figure 27 is the result obtained by measuring the sample structure (iii). The

solid curve In Fig. 27 was obtained in dark room and dash curve was obtained when illuminating the sample with white light source. There is a little bit shift of the transmission pattern which does not resemble Fig. 20. This means the heat effect is not as obvious as in sample (iii).

Figures 28, 29 and 30 are the results of sample from structure (iv). Figure 28 shows the results under dark room condition(solid curve) and under illumination with a white light source (dash curve). Figure 29 shows the results under dark room conditions (solid curve) and under illumination with "blue" laser (He-Cd laser, $\lambda = 0.442\mu m$) (dash curve). Figure 30 shows the symmetry of peaks' positions in dark room condition (solid curve) and under illumination with a "blue" laser (dash curve).

In Figure 31 and 32, the results of sample structure (v) are shown. Figure 31 is the result for a E polarization mode and Figure 28 is the result for an H polarization mode. The transmission intensity for the H mode is larger than that for E - mode which is always true in $\theta \neq 0$ incident angle.

Figure 33 is the result of sample structure (vi). Fig. 33 and Fig. 31, 32 were used to compare with the Conditional Artificial Dielectric Fabry-Perot etalon results with the theory.

Figure 34 is the transmission of light as a function of wavelength through a single layer of CdS on a glass substrate. As can be seen from the graph, an enhanced transmission occurs above $\lambda = 550nm$ signifying the bandgap of the material. Nevertheeless, transmission above that cut-off wavelengyh is not 100 the bandgap of the CdS.

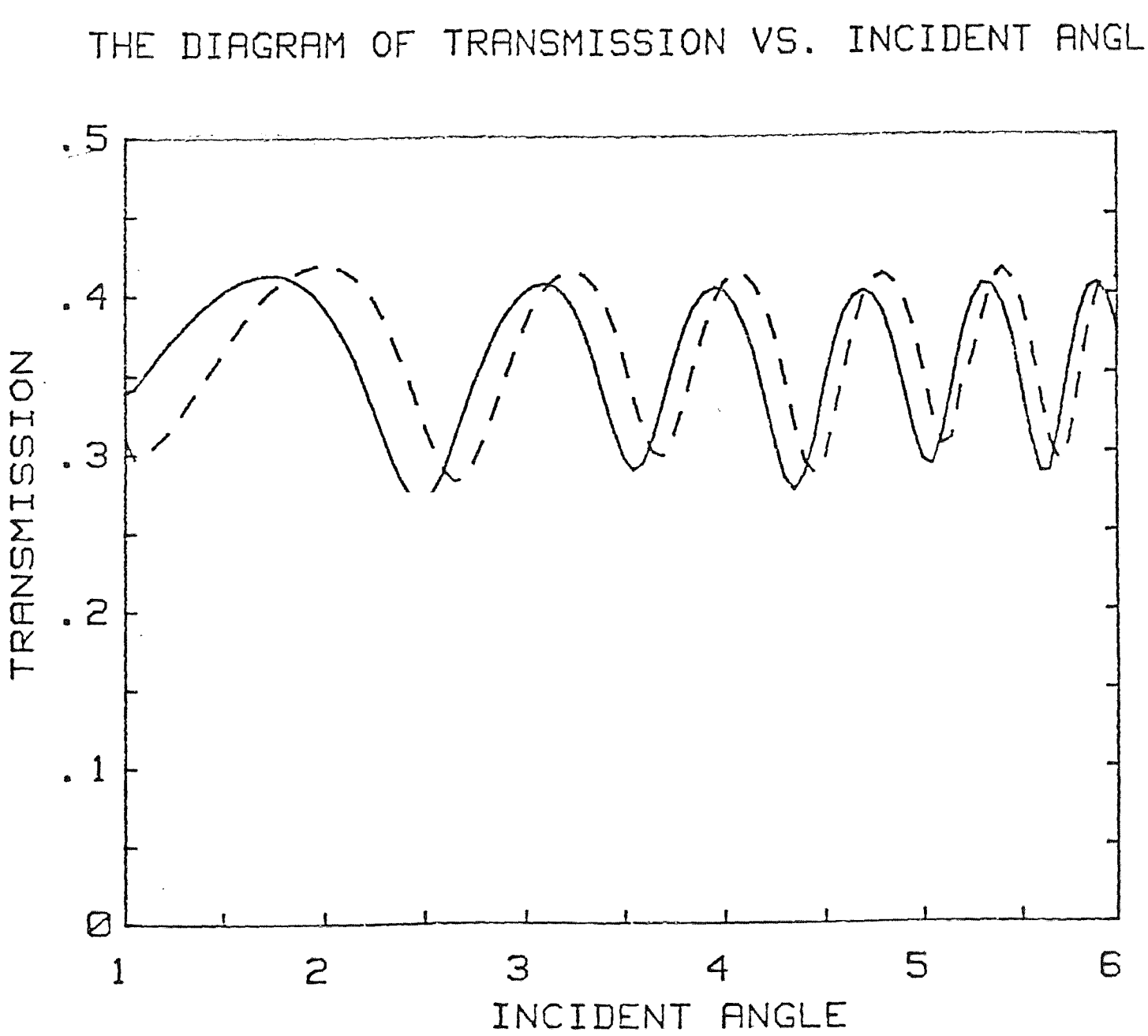

Figure 20a The result of sample structure (i).

—— in dark room. - - - - under illumination of a white light.

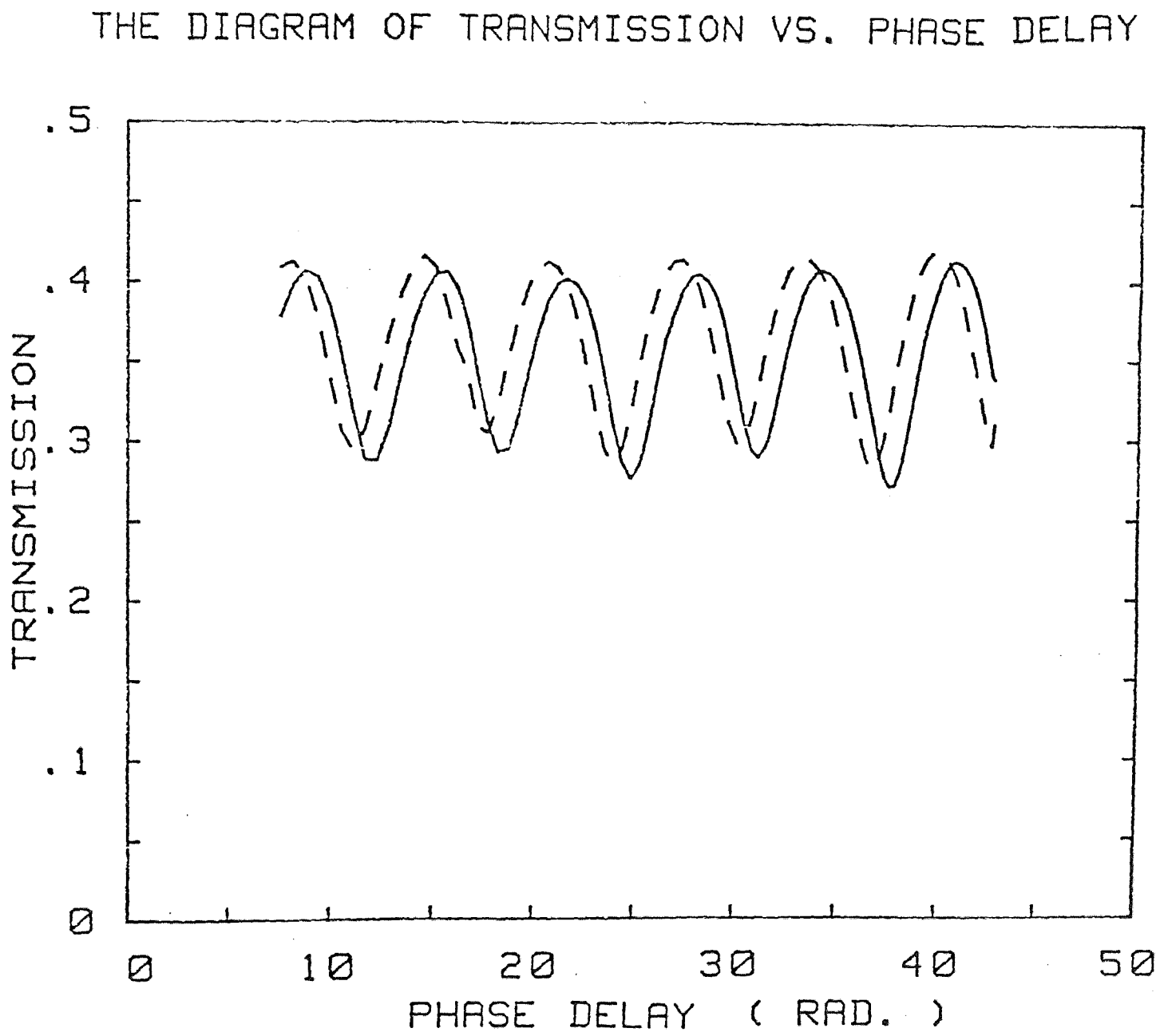

Figure 20b The result of sample structure (i). The figure shows the relation of phase length and transmission.

—— in dark room, - - - - under illumination of a white light.

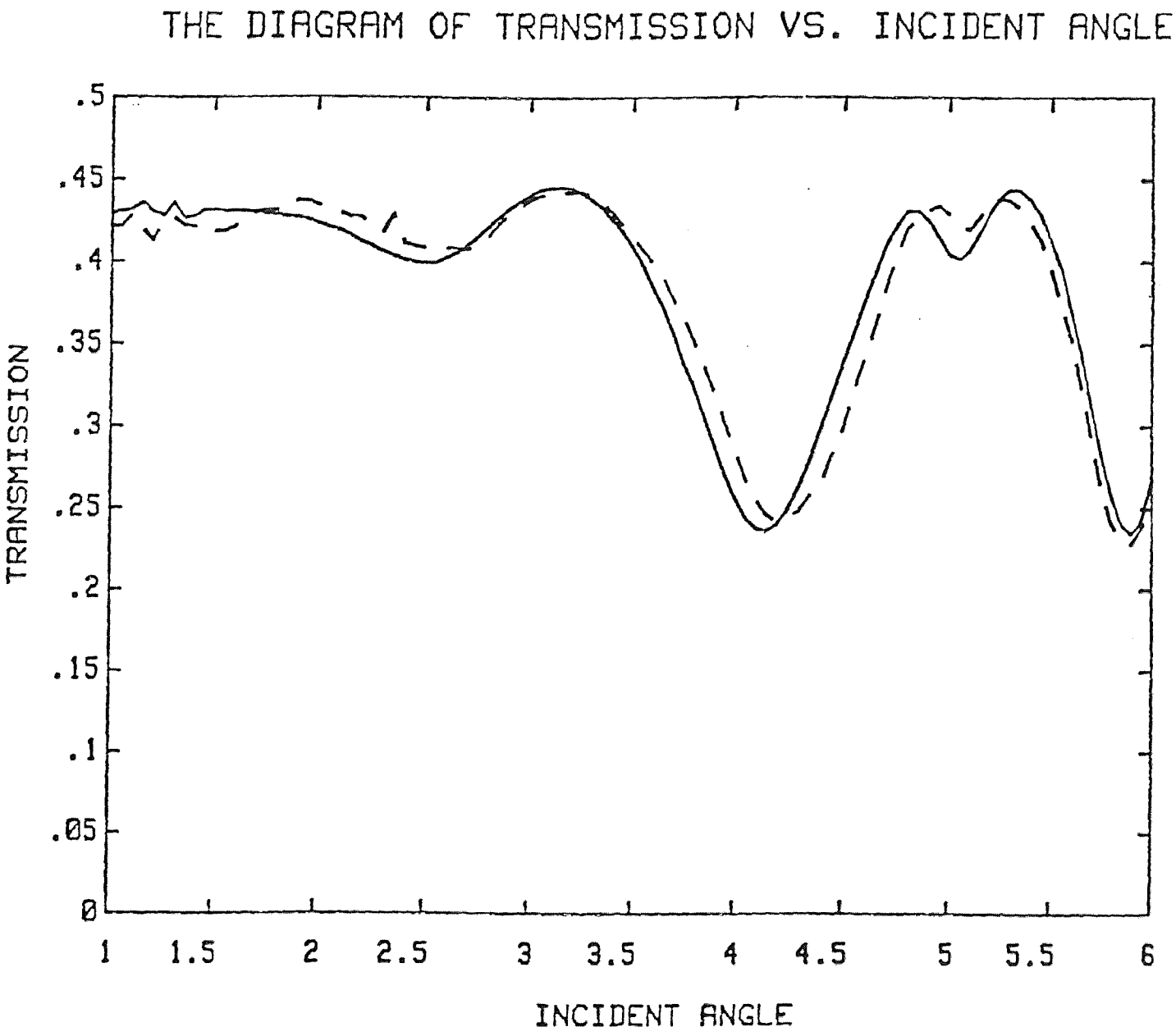

Figure 21 The result of the first sample structure (ii).

—— in dark room, - - - - under illumination of white light.

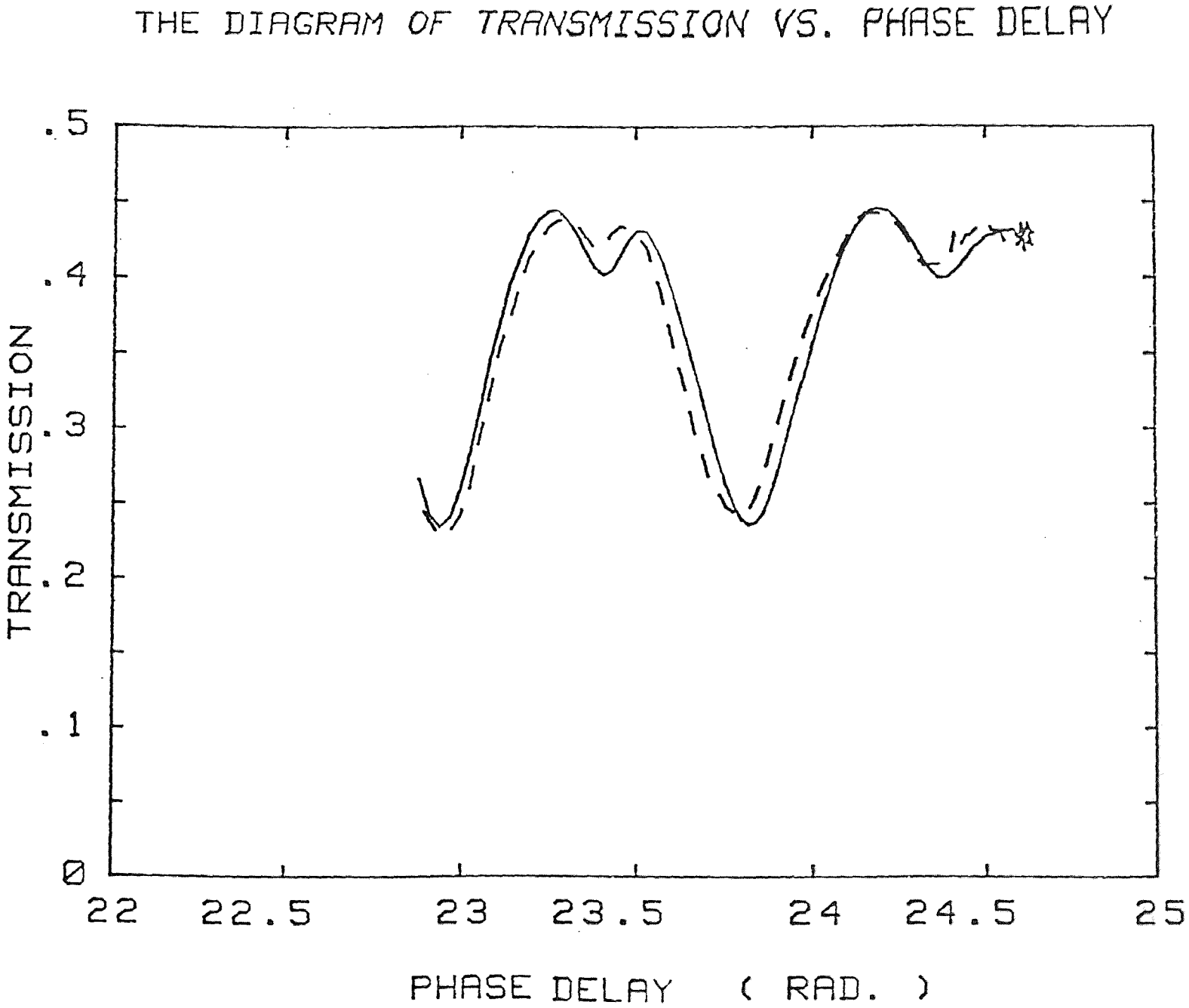

Figure 22 The result of the first sample (ii). The figure is the relation of the phase length and transmission. —— in dark room, - - - - under illumination of white light.

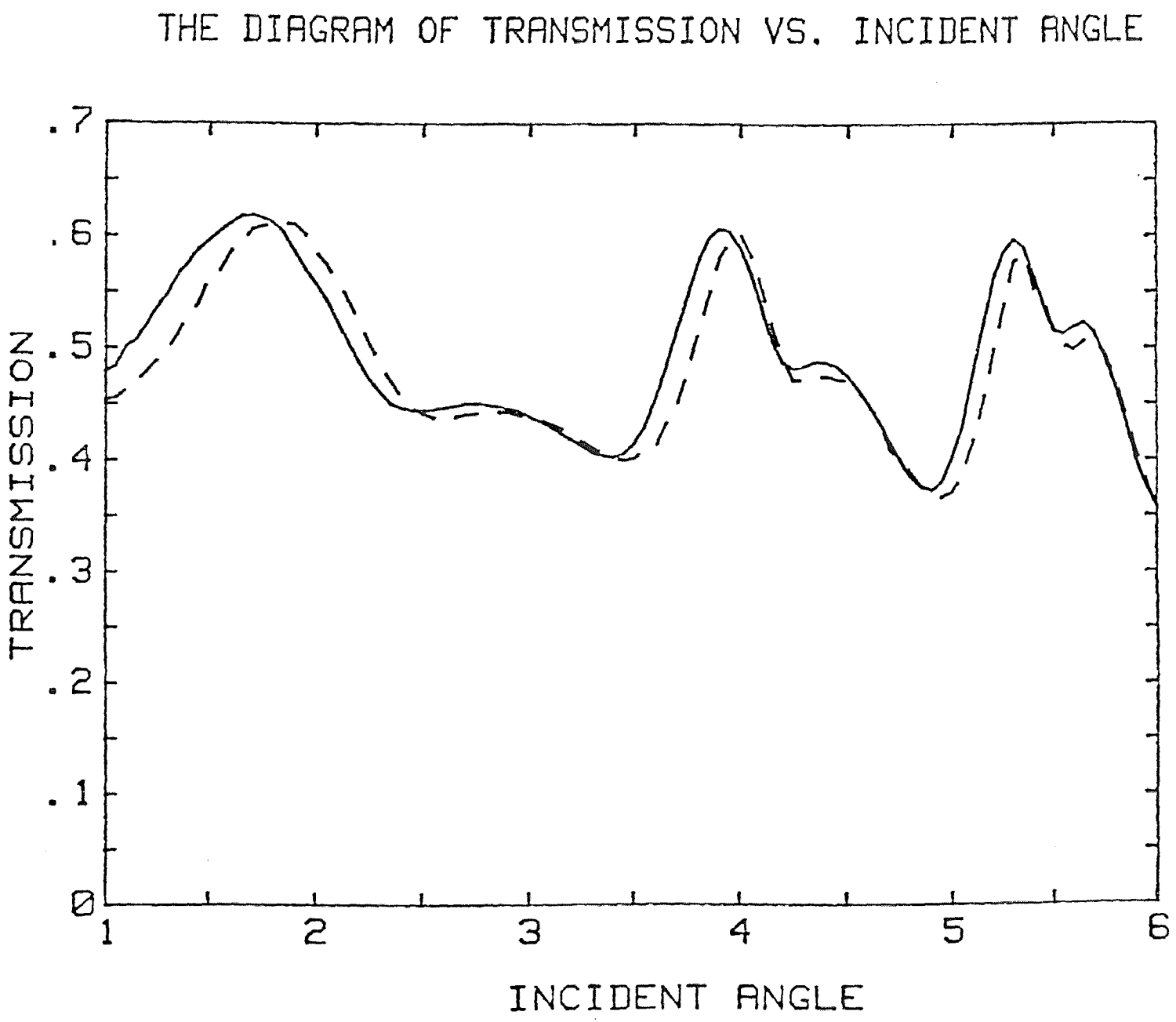

Figure 23 The result of the second sample structure (ii) for H-polarization mode.

—— in dark room, - - - - under illumination of white light.

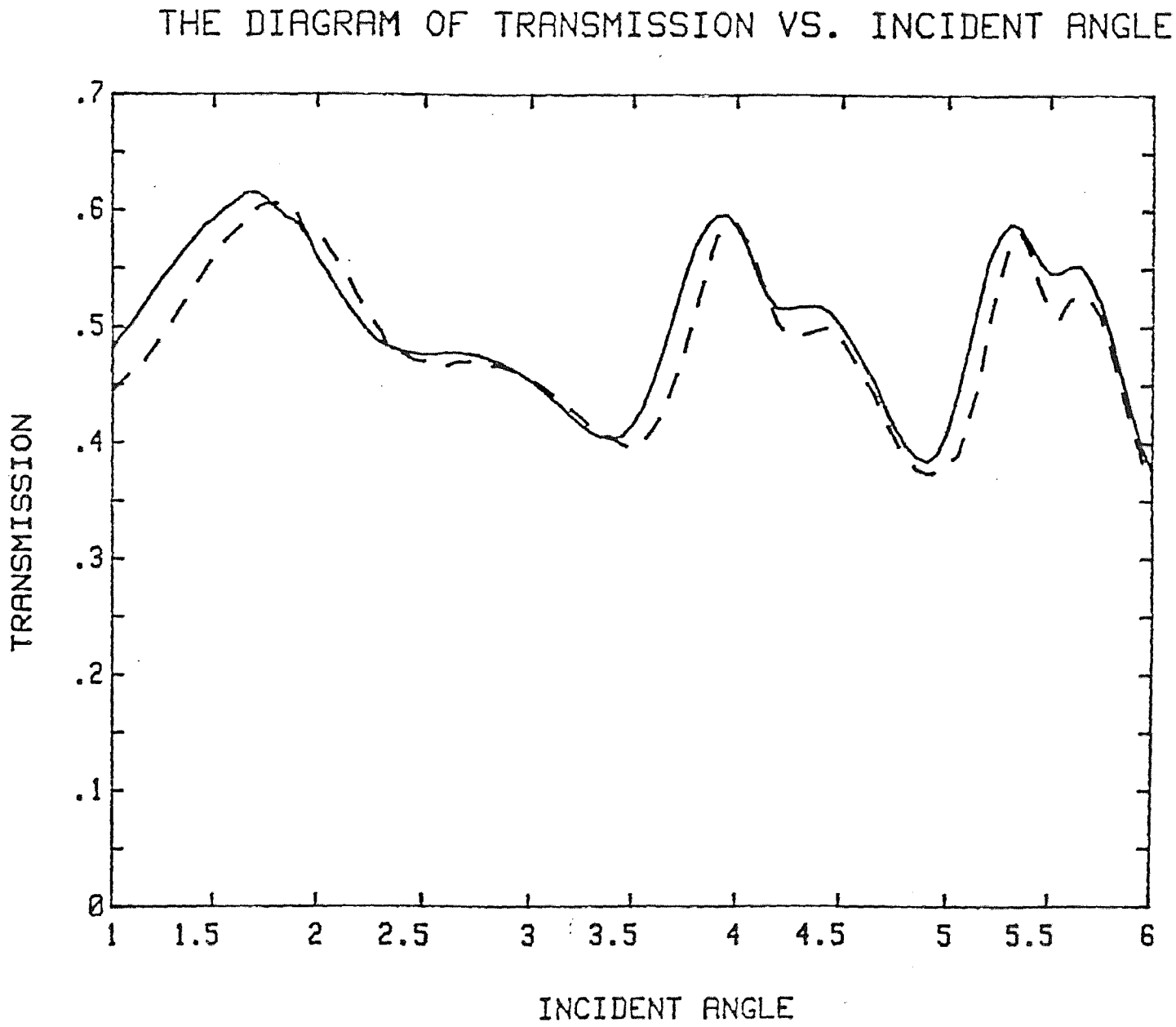

Figure 24 The result of the second sample structure (ii) for E-polarization mode.

—— in dark room, - - - - under illumination of white light.

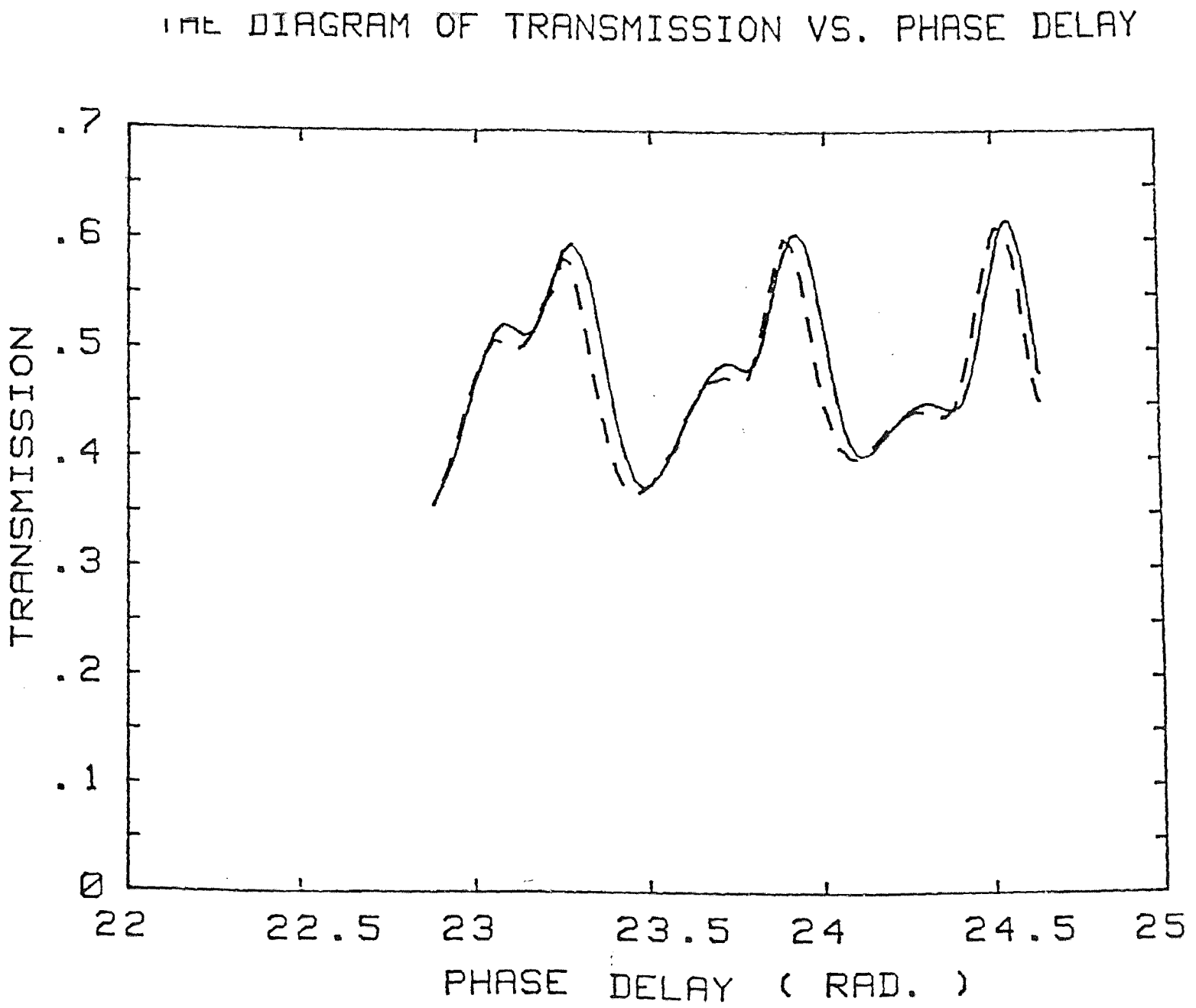

Figure 25 The result of the second sample structure (ii) for H-polarization mode. The figure is the relation of the phase length and transmission.
—— in dark room, - - - - under illumination of white light.

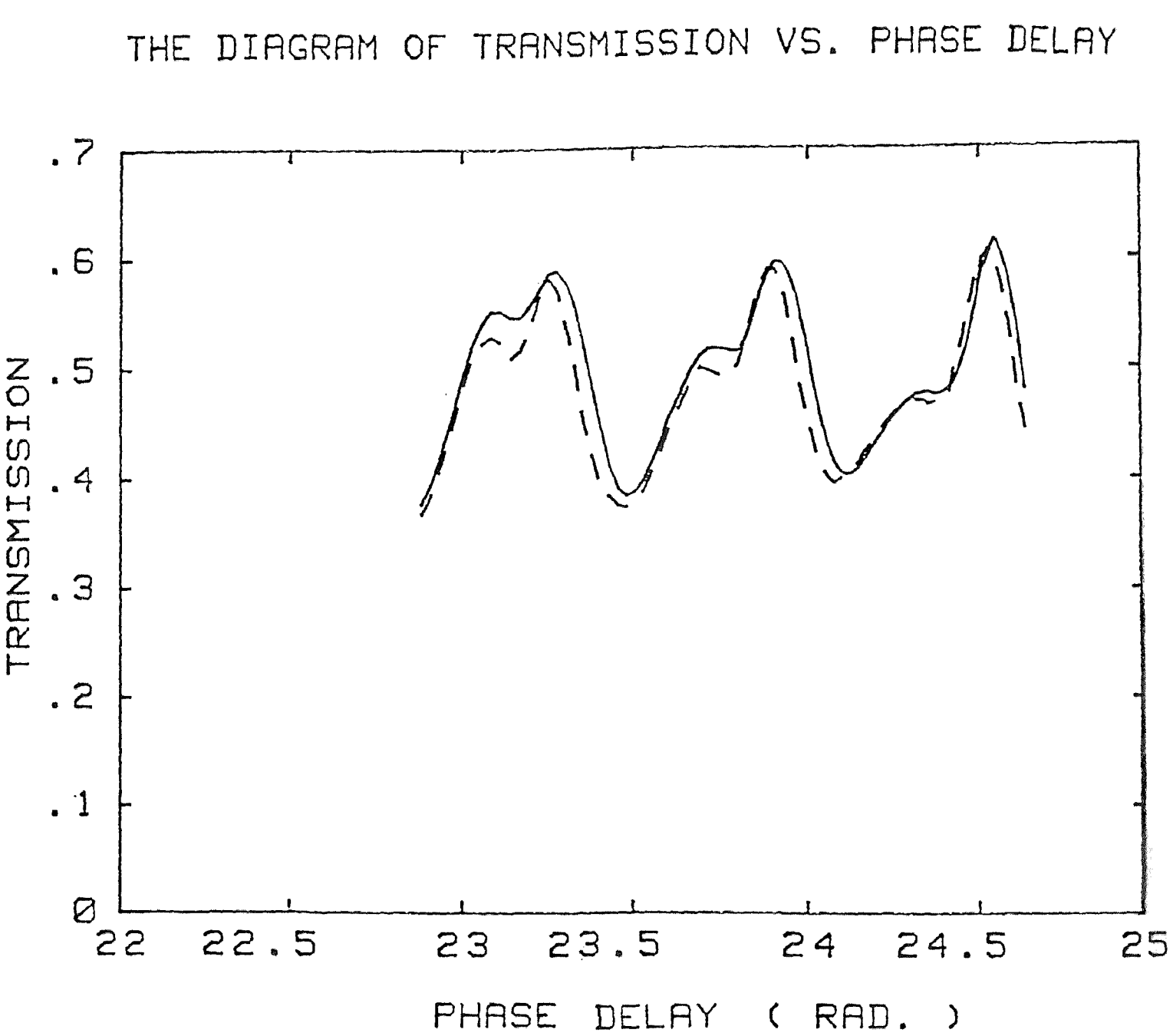

Figure 26 The result of the second sample structure (ii) for E-polarization mode.

The figure is the relation of the phase length and transmission.

—— in dark room, - - - - under illumination of white light.

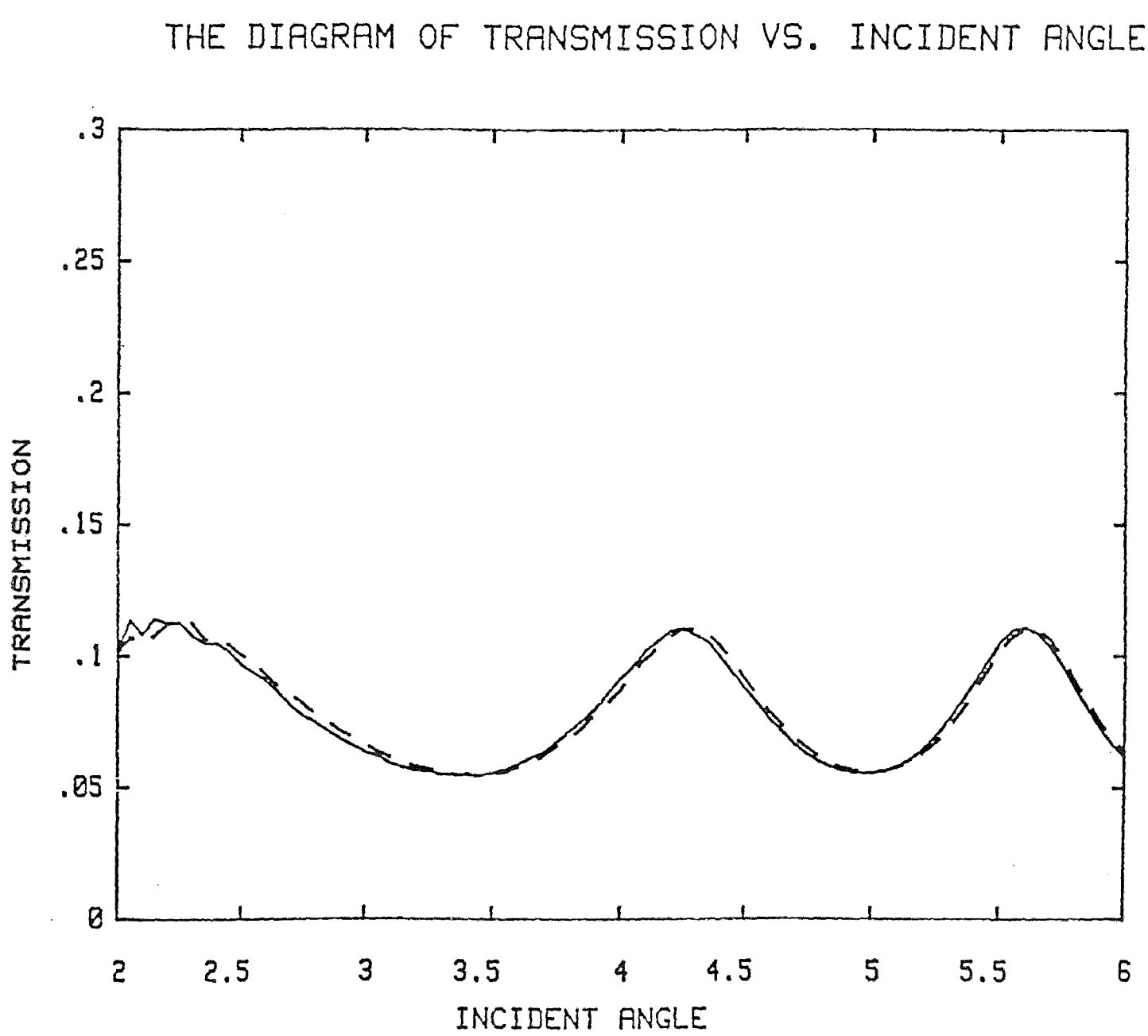

Figure 27 The result of sample structure (iii).

—— in dark room, - - - - under illumination of white light

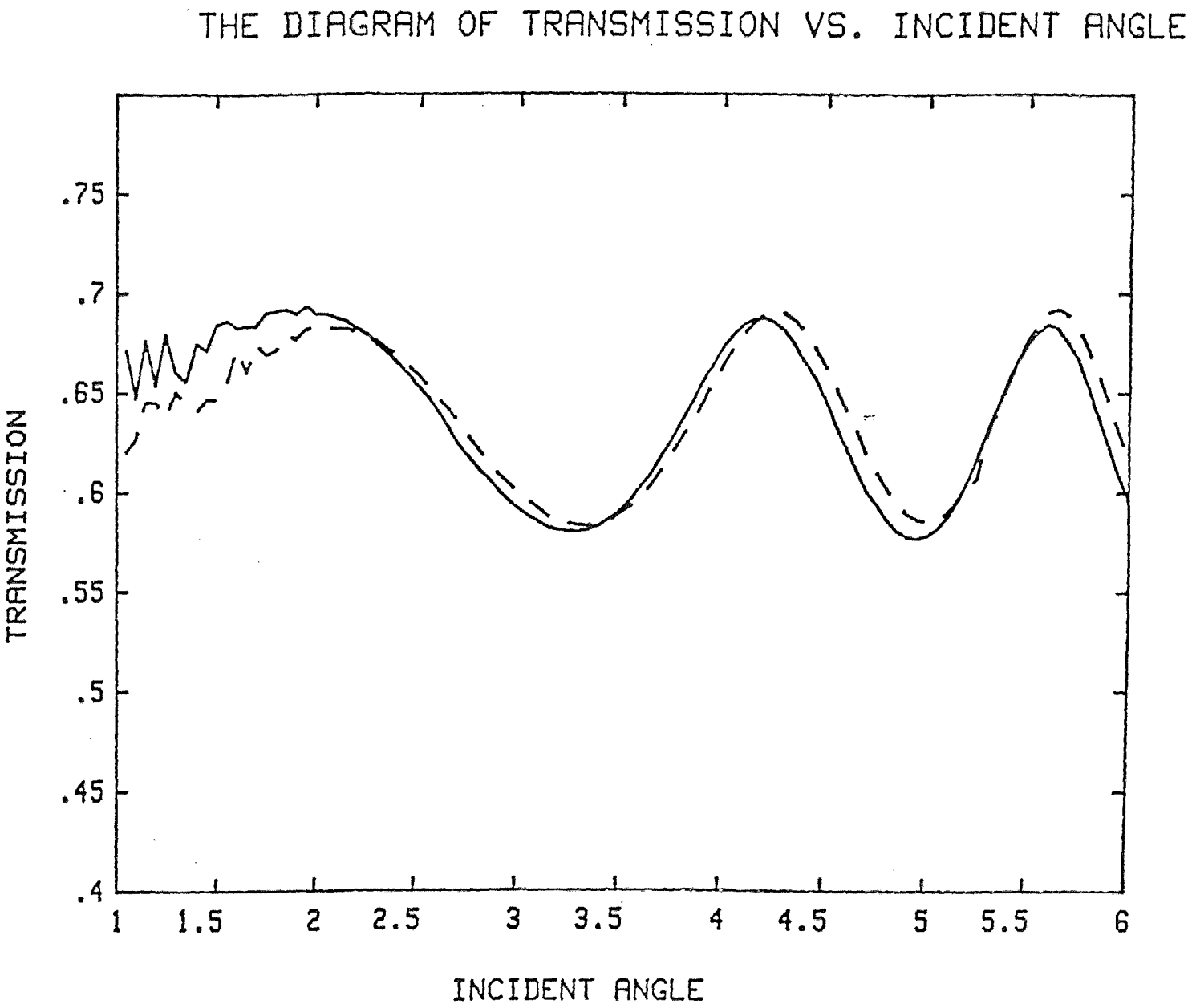

Figure 28 The result of sample structure (iv) for shining white light.

—— in dark room, - - - - under illumination of white light

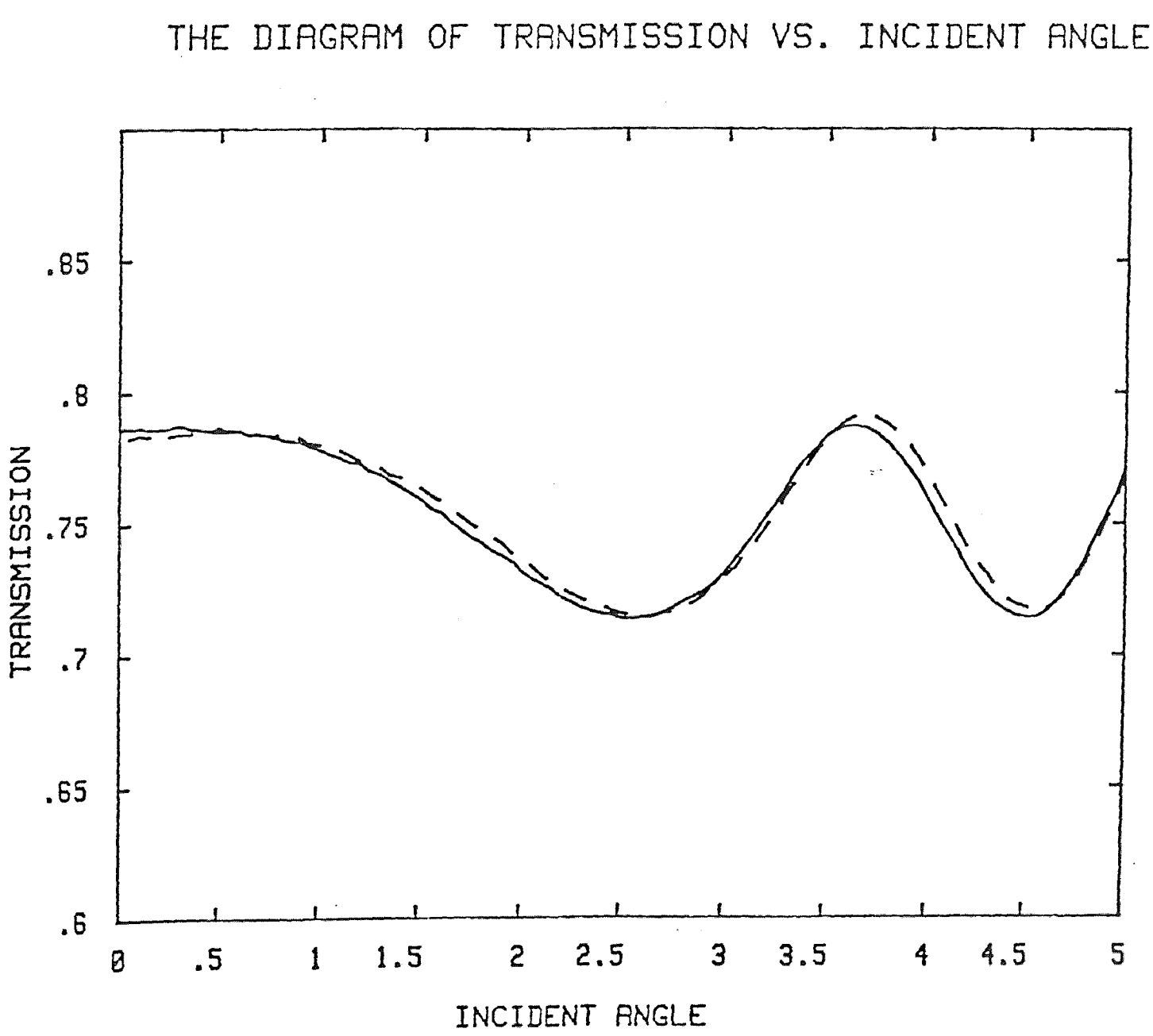

Figure 29 The result of sample (iv) . —— in dark room,

- - - - under illumination of a "blue" laser.

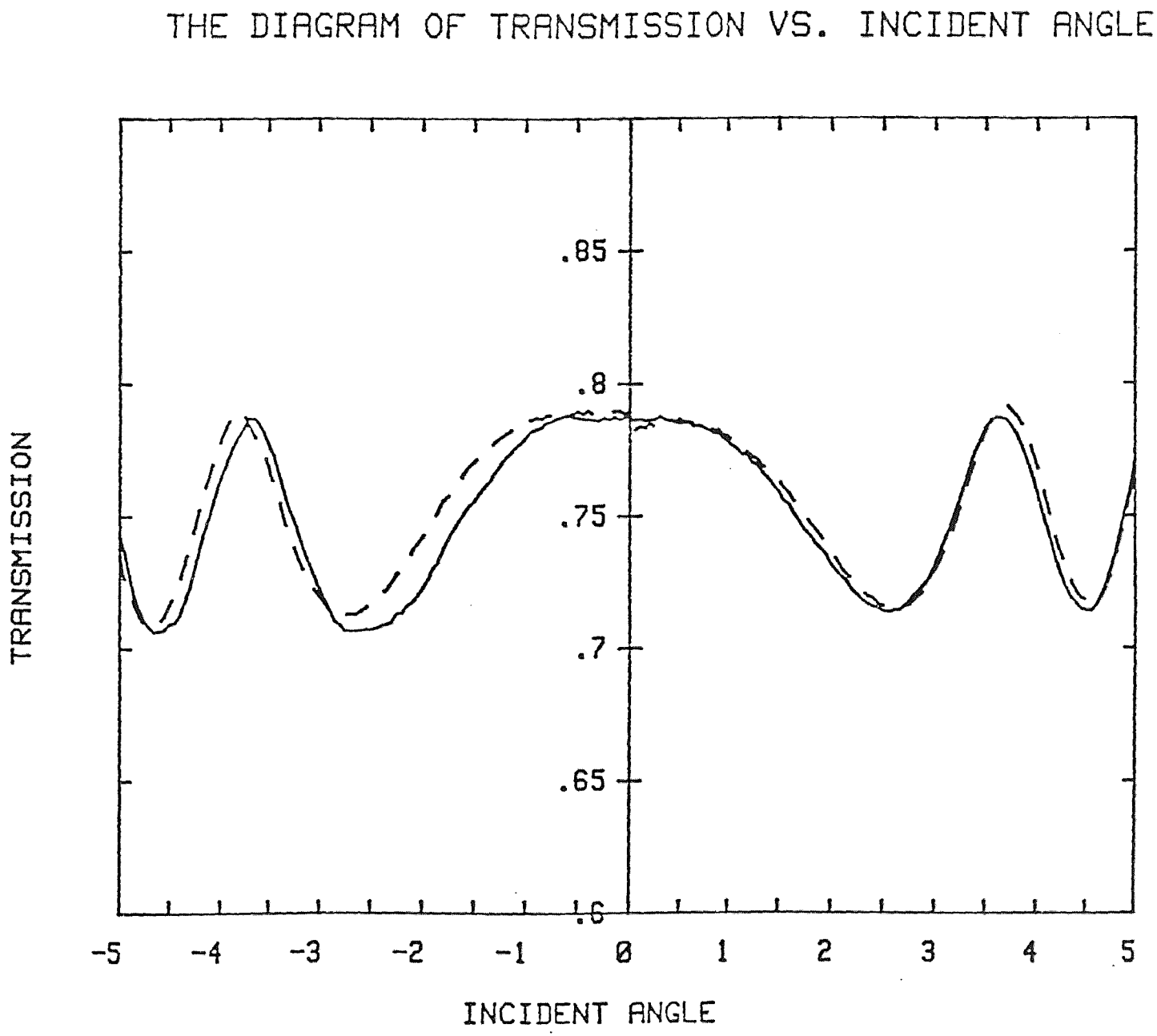

Figure 30 The symmetry of peaks' position for sample structure (iv).
—— in dark room, - - - - under illumination of a "blue" laser

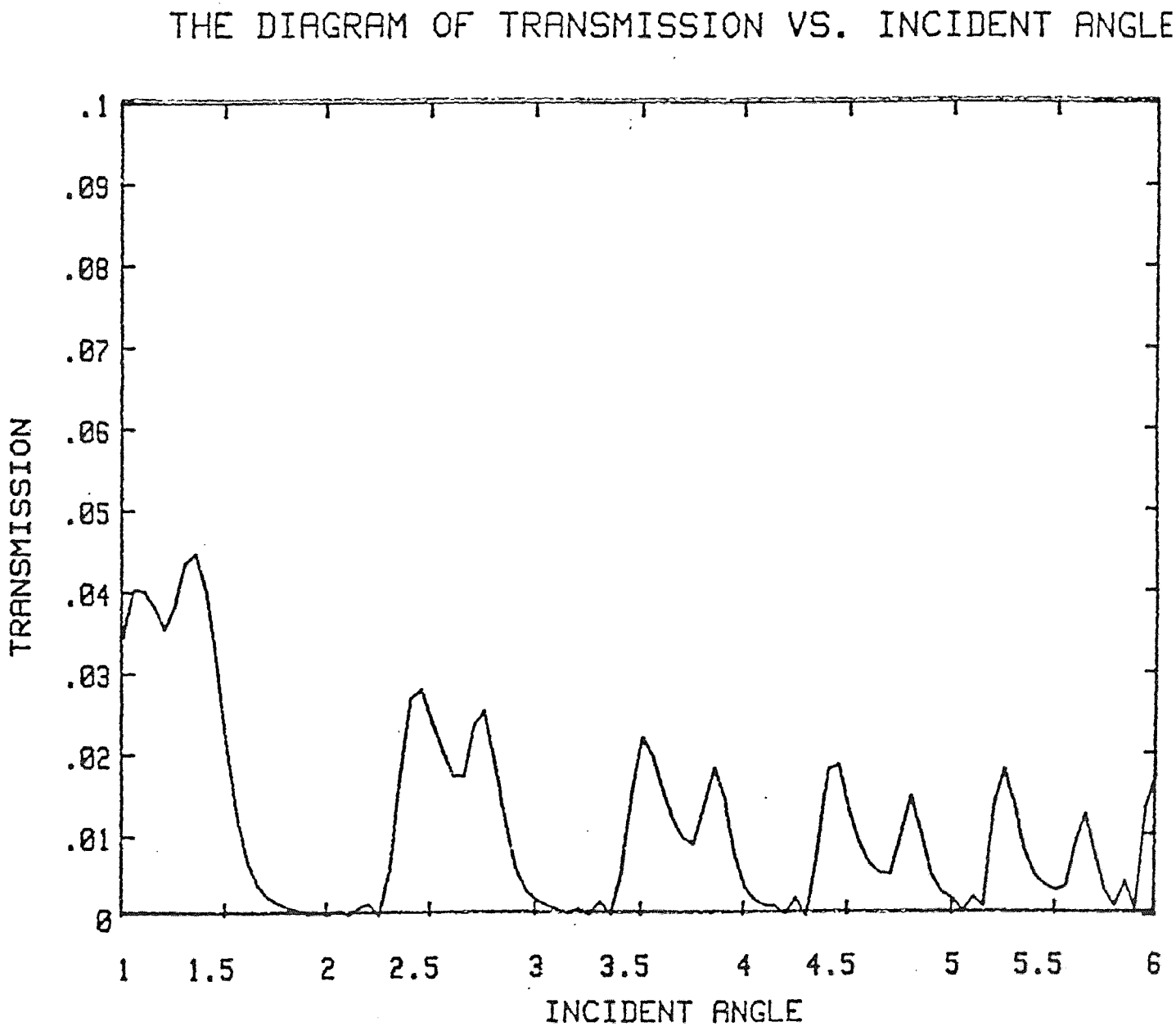

Figure 31 The result of sample structure (v) for E-polarization mode.

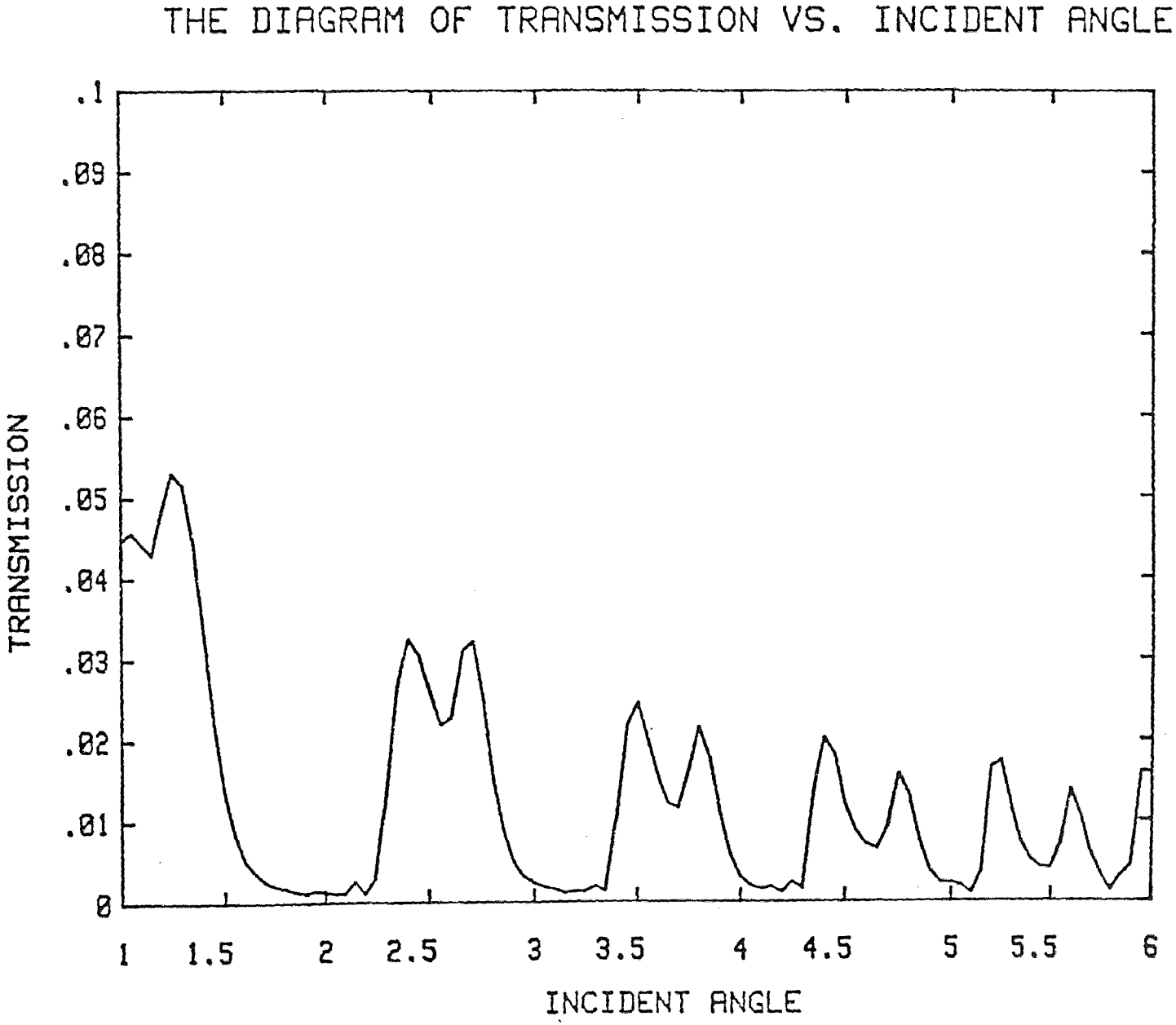

Figure 32 The result of sample structure (v) for H-polarization mode.

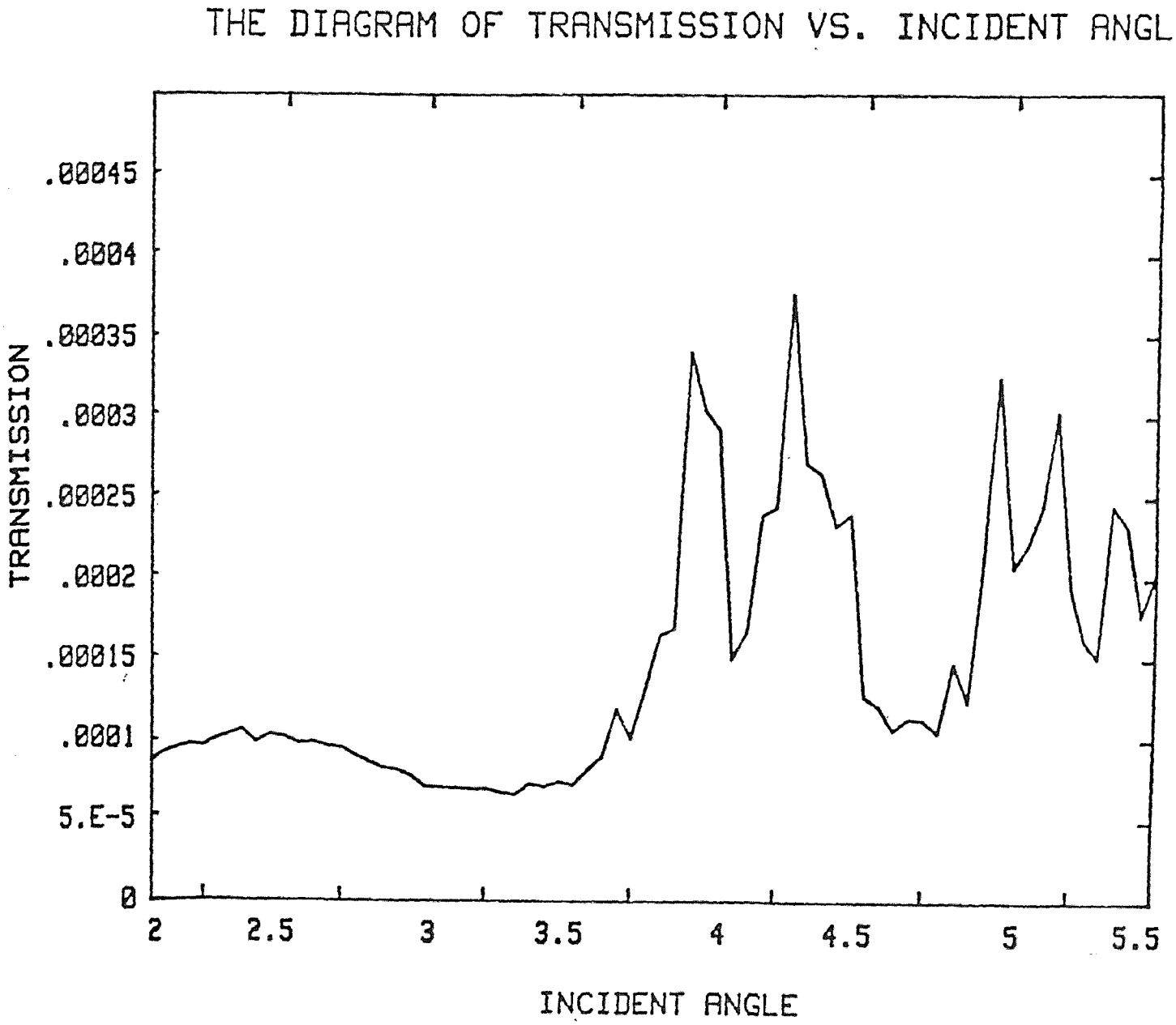

Figure 33 The result of sample structure (vi).

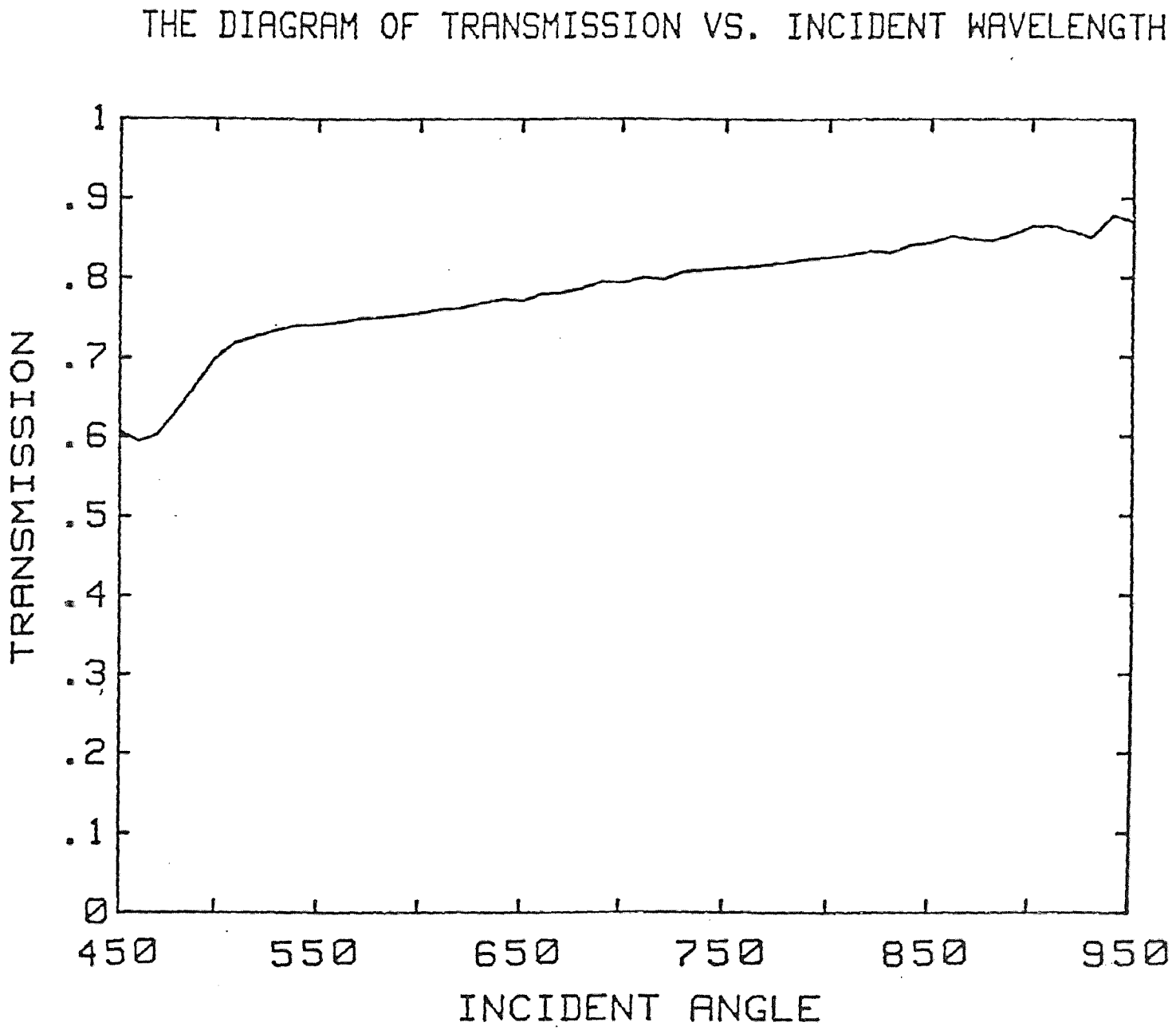

Figure 34 The luminescent effect of CdS thin film in dark room for different wavelength.

5 Discussion

Figures 24 – 29 and 31 – 33 are the experimental results to be compared with the theory (Figures 9 – 14). The first observation is the appearance of a split peak in the experimental results implying the effect of reflection from the photo-sensitive Conditional Artificial Dielectric (CAD) layer. The effect of the layer is also pronounced under no photo-activation (that is without white light illumination or He-Cd laser illumination) implying a scattering loss effect or absorption. Nevertheless, the transmission profile does change with the illumination of the activation source.

As can be seen from Figures 21 – 26 the effect of a white light source or a blue laser illumination is to change the shape of the transmission profile rather than shifting the pattern as demonstrated in Figure 20. We, thus, conclude that the photo-induced effects affect the reflectivity of the middle interface.

Using the sample for which $\phi_1/\phi_2 = 1$, $R_1 = 0.35$ and $R_2 = 0.4$ (sample (ii)), we may calculate the increase of reflectivity in the CAD layer due to the white light source using Figures 9 – 14 as guides. According to these figures, there was

initially some reflectivity of the intermediate layer even in dark condition. We may attribute this initial reflectivity to scattering losses. Assuming that initially this reflectivity value was 1.69 [22] we conclude that the activitating light source (either white light source or the He-Cd laser) increased the reflectivity of the CAD interface by 0.1 and we postulate that this was achieved via the generation of electric and magnetic dipoles in the Conditional Artificial Dielectric layer [11].

6 Conclusion

The Conditional Artificial Dielectrics (CAD) layer was made by depositing CdS clusters on a polymeric matrix. This layer served as a photo-sensitive layer in the middle of a regular, parallel planes Fabry-Perot etalon.

We were able to demonstrate that by embedding this photo-sensitive thin layer in the polymer spacer, we can alter the transmission profile of a Fabry-Perot etalon. This was achieved by photo-inducing changes in the index of refraction. The changes of index of refraction resulted in an enhanced reflection from the layer within the Fabry-Perot leading to changes in the phase of the transmitted beam.

By comparing results from structures with and without the photo-sensitive layer we could estimate the heat effect and determined the relative refractive index change as .01 .

7 Acknowledgements

I would like to thank Dr. H. Grebel sincerely for the completion of the thesis. Owing to his guidence, I can find the clear direction to do my thesis and learn a lot from this experiment. Also I'd like to thank the help and advice from Mr. W. Zhong during this experiment.

References

[1] R. S. Longhurst. *Geometrical and Physical Optics.* 3rd Ed., Longman Group Limited, 1973.

[2] P. Jacquinot. *The Luminosity of Spectrometers with Prisms, Gratings or Fabry-Perot Etalons.* J. Opt. Soc. Am., 44, 761, 1954.

[3] G. Hernandez. *Analytical Description of a Fabry-Perot Spectrometer : Optimum Operation with a Spherical Etalon.* Applied Optics, Vol. 24, No. 22, Nov. 1985.

[4] H. Grebel, P. Chen. *Artificial Dielectric Polymeric Waveguides : Semiconductor-Embedded Films.* Opt. Lett., Vol. 15, No. 12, PP. 667-669, Jun. 15 1990.

[5] H. Ho. *Conditional Artificial Dielectric Waveguide.* Master thesis, NJIT, 1990.

[6] C. F. McMilan. *Fabry-Perot Misalignment : The Effect on Peak Position.* Appl. Optics, Vol. 25, No. 16, PP. 2785 – 2789, 15 Aug. 1986.

[7] H. Yasuda , C. E. Lamaze. *Polymerization in an Electrodeless Glow Discharge. II. Olefinic Monomers.* J. of Appl. Polymer Sci., Vol. 17, PP.1519 – 1531, 1973.

[8] H. Yasuda, T. Hirotsu. *Distribution of Polymer Deposition in Plasma Polymerization. I. Acetylene, Ethylene, and the Effect of Carrier Gas.* J. of Polymer Sci. : Polymer Chemistry Edition, Vol. 16, PP. 229 – 241, 1978.

[9] C. A. Eidering, A. Knoesen, S. T. Kowel. *Use of Fabry-Perot Device for the Characterization of Polymeric Electro- optic Films.* J. Appl. Phys. Vol. 69, PP.3676 – 3686, 15 Mar. 1991.

[10] I. Prikryl. *Analytical Description of an Imperfect Fabry-Perot Etalon.* Appl. Optics, Vol. 23, No. 4, PP. 621 – 626, 15 Feb. 1984.

[11] I. J. Ferrer, P. Salvador. *Photoluminescence and Electroluminescence Mechanisms at Polycrystalline CdS in Air and in Contact with Aqueous Electrolytes.* J. Appl. Phys., Vol 66 (6), PP. 2568 – 2577, 15 Sep. 1989.

[12] H. van de Stadt, J. M. Muller. *Multimirror Fabry-Perot Interferometers.* Opt. Sci. Am., Vol. 2, No. 8, PP. 1363 – 1370, Aug. 1985.

[13] M. Born, E. Wolf. *Principles of Optics.* 2nd Edi., New York, The MacMillan Co., 1964.

[14] A. Yariv. *Optical Electronics.* 3rd Edi., Library of Congress Cataloging in Publication Data, 1985.

[15] F. G. Smith, J. H. Thomson. *Optics.* 2nd Edi., John Wiley & Sons Ltd., 1988.

[16] M. V. Klein, T. E. Furtak. *Optics* 2nd Edi., Library of Congress Cataloging in Publication Data, 1986.

[17] C. A. Balanis. *Advanced Engineering Electromaganetics.* John Wiley & Sons, Inc., 1989.

[18] E. Hecht, A. Zajac. *Optics.* Addison - Wesley Publishing Co., 1985.

[19] G. Hernandez. *Fabry-Perot With an Absorbing Etalon Cavity.* Appl. Opt., Vol. 24, No. 18, PP. 3062 – 3067, 15 Sep. 1985.

[20] C. A. Eldering, S. T. Kowel, A. Knoesen. *Electrically Induced Transmissivity Modulation in Polymeric Thin Film Fabry-Perot Etalons.* Appl. Optics, Vol. 28, No. 20, PP. 4442 – 4445, 15 Oct. 1989.

[21] H. M. Tong, H. K. D. Hsuen, K. L. Saenger. *Thickness-Direction Coefficient of Thermal Expansion Measurement of Thin Polymer Films.* Rev. Sci. Instrum., Vol. 62 (2), Feb. 1991.

[22] H. Jerominek, M. Pigeon, S. Patela, Z. Jakubozyk, C. Delisle. *CdS Microcrystallites-Doped Thin-Film Glass Waveguides.* J. Appl. Phys., Vol. 63, No. 3, Feb. 1988.

[23] J. B. Kumer, T. C. James. *Effect of Substrate Absorption on the Performance of Solid Fabry-Perot Etalons.* Appl. Optics, Vol. 27, No. 23, 1 Dec. 1988.

[24] G. F. D'Alelio, A. B., Ph.D.. *Fundamental Principles of Polymerization. Rubber, Plastics and Fibers* . John Wiley & Sons, Inc., 1952.

[25] H. Yasuda. *Plasma Polymerization* . Academic Press, New York, 1985.

[26] L. Holland. *Vacuum Deposition of Thin Films* . John Wiley & Sons Inc., 1958.

[27] E. R. Blout, H. Mark. *Monomers.* Interscience Publishers Inc., 1949.

[28] H. A. Macleod. *Thin-Film Optical Filters.* 2nd Ed., Macmillan Publishing Company, 1986.

[29] L. Levi. *Applied Optics A Guide to Optical System Design.* Vol. 2, John Wiley & Sons, 1980.